Langtaosha (LTS) Preprint doi: https://doi.org/10.65215/LTSpreprints.2026.08.25.000317. This version posted August 26, 2026. The copyright holder for this preprint (which was not certified by peer review) is the author/funder. Creative Commons license: CC Attribution-NonCommercial-NoDerivatives 4.0 https://creativecommons.org/licenses/by-nc-nd/4.0

Title: Signaling center-guided human gastruloids progress toward early organogenesis

Author information

Bin Wang[1,2,3,4,11], Hanwen Yu[1,2,3,11], Ruiyang Li[1,2,3,11], Junhua Chen[1,2,3,11], Wenjin Ye[1,2,3,11], Xiaoyu Wang[7,11], Dairui Li[1,2,3], Huanyao Liu[1,2], Jierui Chen[1,2], Yili Wei[1,2,3], Shanshan Huang[1,2,3], Lan Wei[1,2,3], Zihao Li[1,2,3], Chaoying Wen[1,2,3], Jiacheng Deng[1,2], Qiumin Chen[1,2], Tao Wang[1,2,3], Zhipeng Tan[1,2,3], Dongjun Lin[4], Bruce T. Lahn[1,10], Lili Chen[5,6,*], Jichang Wang[1,2,3,8,9,*], Andy Peng Xiang[1,2,3,*], Weiqiang Li[1,2,3,12,*]

Affiliations information

[1]Center for Stem Cell Biology and Tissue Engineering, Key Laboratory for Stem Cells and Tissue Engineering, Ministry of Education, Sun Yat-sen University, Guangzhou, Guangdong, China

[2]National-Local Joint Engineering Research Center for Stem Cells and Regenerative Medicine, Zhongshan School of Medicine, Sun Yat-sen University, Guangzhou, Guangdong, China

[3]Department of Histology and Embryology, Zhongshan School of Medicine, Sun Yat-sen University, Guangzhou, Guangdong, China

[4]Department of Hematology, The Seventh Affiliated Hospital, Sun Yat-sen University, Shenzhen, Guangdong, China

[5]Hospital of Stomatology, Guanghua School of Stomatology, Sun Yat-sen University, Guangzhou, China

[6]Guangdong Provincial Key Laboratory of Stomatology, Guangzhou, China

[7]Division of Histology & Embryology, Key Laboratory for Regenerative Medicine of the Ministry of Education, College of Medicine, Jinan University, Guangzhou, Guangdong, China

[8]Advanced Medical Technology Center, The First Affiliated Hospital, Zhongshan School of Medicine, Sun Yat-sen University, Guangzhou, Guangdong, China

[9]Reproductive Medicine Center, The First Affiliated Hospital, Sun Yat-sen University, Guangzhou, Guangdong, China

[10]Department of Human Genetics, University of Chicago, Chicago, IL 60637, USA

[11]These authors contributed equally

[12]Lead contact

*Correspondence: chenlili555@mail.sysu.edu.cn (L.C.)
wangjch53@mail.sysu.edu.cn (J.W.);
xiangp@mail.sysu.edu.cn (A.P.X.);
liweiq6@mail.sysu.edu.cn (W.L.)

Langtaosha (LTS) Preprint doi: https://doi.org/10.65215/LTSpreprints.2026.08.25.000317. This version posted August 26, 2026. The copyright holder for this preprint (which was not certified by peer review) is the author/funder. Creative Commons license: CC Attribution-NonCommercial-NoDerivatives 4.0 https://creativecommons.org/licenses/by-nc-nd/4.0

Graphical abstract

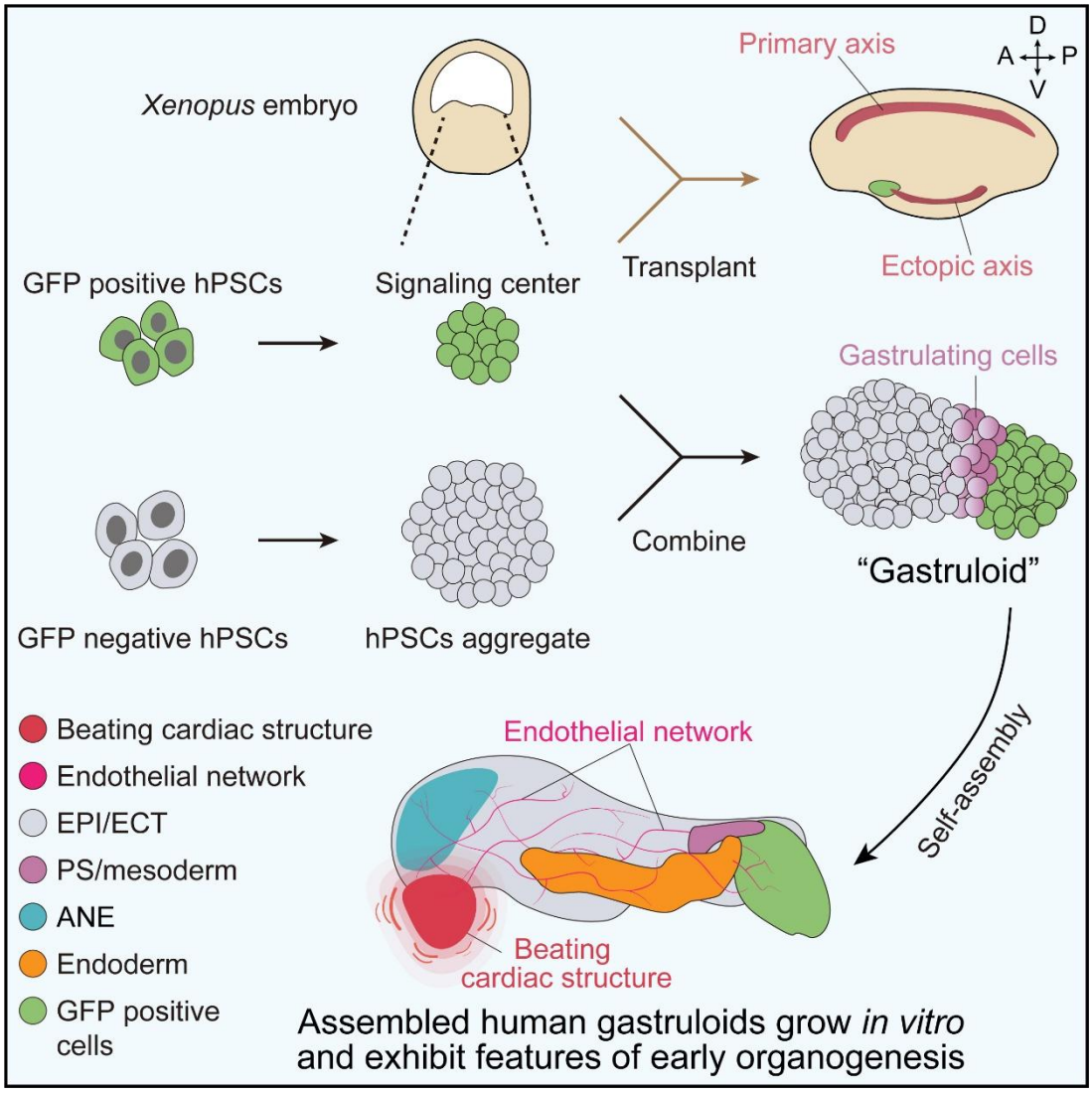

Highlights

- A WNT/NODAL-induced signaling center drives human gastruloid self-organization
- The model progresses from gastrulation toward early organogenic development
- The model exhibits neural, cardiac-like, and endothelial-associated features without exogenous lineage-specific signals
- Single-cell analysis maps emerging cell populations onto human developmental references

In brief

A WNT/NODAL-induced signaling center drives human gastruloid self-

Langtaosha (LTS) Preprint doi: https://doi.org/10.65215/LTSpreprints.2026.08.25.000317. This version posted August 26, 2026. The copyright holder for this preprint (which was not certified by peer review) is the author/funder. Creative Commons license: CC Attribution-NonCommercial-NoDerivatives 4.0 https://creativecommons.org/licenses/by-nc-nd/4.0

organization and progression beyond gastrulation toward early organogenic development, including neural tissues, cardiac-like structures, and nascent endothelial networks.

Abstract

The transition from gastrulation to early organogenesis represents a pivotal milestone in embryogenesis, yet remains poorly understood due to limited access to human models. Inspired by the organizing activity of signaling centers in embryonic development, including the Spemann-Mangold organizer, we present a self-organizing human gastruloid model driven by a WNT/NODAL-induced signaling center. With minimal external input, this center triggers a developmental cascade involving anterior-posterior symmetry breaking, axial elongation, and germ layer specification. Upon extended culture, the model exhibits early organogenic features, including neural development, and the spontaneous co-emergence of contractile cardiac-like structures accompanied by primitive endothelial networks. Single-cell RNA sequencing maps the model's cell populations onto human developmental references spanning gastrulation and early organogenesis. By re-emphasizing signaling asymmetry as an organizing principle, this platform provides a simple, ethically compliant, and experimentally tractable window into early multilineage organogenesis and enables investigation of how signaling centers contribute to human developmental patterning.

Introduction

The specification of the three primary germ layers—ectoderm, mesoderm, and endoderm—initiates morphofunctional organization that gives rise to organ primordia during the third and fourth weeks after human fertilization[1,2]. Despite its fundamental importance, this developmental continuum remains difficult to interrogate directly, owing to ethical constraints such as the 14-day rule[3], and interspecies divergences that complicate the extrapolation of animal studies to humans[4,5]. Consequently, human pluripotent stem cell (hPSC)-derived embryo models have emerged as a promising platform for probing early embryogenesis[6,7]. Systems including blastoids[8-11], post-implantation embryo models[12-19], and gastruloids[20,21] have recapitulated key aspects of lineage specification and morphogenesis from pre-implantation stages through gastrulation. However, most existing human embryo models often reach a developmental plateau shortly after initial lineage specification and exhibit limited capacity to autonomously sustain the coordinated, tissue-level

Langtaosha (LTS) Preprint doi: https://doi.org/10.65215/LTSpreprints.2026.08.25.000317. This version posted August 26, 2026. The copyright holder for this preprint (which was not certified by peer review) is the author/funder. Creative Commons license: CC Attribution-NonCommercial-NoDerivatives 4.0 https://creativecommons.org/licenses/by-nc-nd/4.0

morphogenesis required for progression beyond gastrulation toward early organogenesis[22].

To overcome this hurdle, current advanced models typically rely on the sequential and global administration of morphogens to guide development through discrete stages[23-33]. While these approaches efficiently generate defined cell types, including cardiomyocytes and neural progenitors, they rely on spatially uniform signaling conditions, which may only partially recapitulate the intrinsic patterning logic of the embryo[34]. *In vivo*, embryonic patterning is governed not by homogeneous exposure to signaling factors, but by spatiotemporally restricted signaling centers that establish morphogen gradients and positional information[35]. The Spemann-Mangold organizer exemplifies this principle as a localized hub that orchestrates axial patterning, organizes germ layers, and demarcates organ fields[36,37]. Reconstituting this form of spatially confined signaling in human *in vitro* systems remains challenging, as isolated hPSC aggregates struggle to establish and sustain robust, directional morphogen gradients required for continuous developmental progression. Although engineered strategies, such as microfluidic platforms, optogenetic control, and DNA-programmed assembly, can successfully impose spatial patterning, their technical complexity may limit scalability, and their reliance on external manipulation could introduce variability affecting subsequent developmental outcomes[38-41].

Here, we establish a human embryo-like model that develops autonomously under the control of a spatial hPSC-derived signaling center. Building on insights from vertebrate organizer biology, we engineered a minimal signaling hub via the transient co-activation of the WNT and NODAL pathways[37,42,43]. Upon physical integration with an uninstructed hPSC aggregate, this center triggers a robust and self-sustaining developmental cascade, including symmetry breaking, axial elongation, and germ layer deployment, in the absence of staged media changes, exogenous scaffolds, or additional patterning cues. Crucially, these signaling center-guided gastruloids further exhibited developmental continuity beyond gastrulation, with features of early organogenesis including neural development and spontaneously contracting cardiac-like tissues accompanied by extensive endothelial-like networks. Single-cell transcriptomic analyses revealed cell states corresponding to human gastrulation followed by progressive emergence of transcriptional programs associated with early organogenesis[44-47].

In summary, our findings show that a WNT/NODAL-induced signaling center promotes self-organization of human gastruloids, enabling their

Langtaosha (LTS) Preprint doi: https://doi.org/10.65215/LTSpreprints.2026.08.25.000317. This version posted August 26, 2026. The copyright holder for this preprint (which was not certified by peer review) is the author/funder. Creative Commons license: CC Attribution-NonCommercial-NoDerivatives 4.0 https://creativecommons.org/licenses/by-nc-nd/4.0

progression beyond gastrulation toward early organogenic development *in vitro*. By reinstating signaling asymmetry as a central organizing principle, this system provides a tractable platform to interrogate how signaling centers orchestrate human embryogenesis beyond gastrulation, an otherwise inaccessible developmental process.

Results

Generation of a signaling center from human pluripotent stem cells

Building on evidence that combining WNT/NODAL activation confers embryonic patterning-guided ability to hPSC derivatives[48], we first formed 3D spheroids by culturing GFP-positive H1 hPSC in AggreWell plates and treating them with CHIR (a WNT agonist)[49] and Activin A (a NODAL agonist)[50] (Figures 1A and 1B). To functionally validate the signaling center, we transplanted these cells into *Xenopus* embryos using an established protocol[51] (Figure 1C). Remarkably, embryos receiving instructed hPSCs developed ventral protrusions, unlike control embryos transplanted with basic medium (control) or untreated hPSCs (Figures S1A and S1B). Immunofluorescence (IF) analysis revealed ectopic SOX2-positive neural structures on the ventral side, formed by GFP-negative host-derived cells adjacent to GFP-positive cells (Figure 1C). Histological examination further identified two distinct neural domains: the endogenous dorsal neural tube and the induced ventral ectopic tissues, both expressing SOX2 and PAX6 (Figures S1C-S1E). Moreover, the instructed cells expressed key organizer markers, including GSC, FOXA2, and NOGGIN (Figures S1F and S1G). These findings indicate that WNT/NODAL activation establishes a signaling state with embryonic inductive activity, capable of influencing surrounding embryonic tissue patterning[52,53].

Construction of a signaling center-guided model

In a parallel experiment, GFP-negative H1 hPSC cultured in 96-well low-attachment plates using serum-free N2B27-supplemented medium formed spherical aggregates within 24 hours while maintaining pluripotency markers OCT4, SOX2, and NANOG (Figures 1D-1F). To introduce a localized signaling hub, we assembled these pre-formed GFP-negative hPSC aggregates with CHIR/Activin A-treated GFP-hPSC, and cultured the assemblies in basal medium without additional exogenous factors (Figure 1G). By day 5, experimental assemblies containing GFP-positive signaling centers consistently exhibited elongated morphologies across multiple batches, whereas control assemblies with untreated GFP-hPSC remained uniform

Langtaosha (LTS) Preprint doi: https://doi.org/10.65215/LTSpreprints.2026.08.25.000317. This version posted August 26, 2026. The copyright holder for this preprint (which was not certified by peer review) is the author/funder. Creative Commons license: CC Attribution-NonCommercial-NoDerivatives 4.0 https://creativecommons.org/licenses/by-nc-nd/4.0

spheroids (Figures 1G-1I, S2A, S2B, S3, and Video S1). Notably, neither isolated hPSC aggregates nor signaling centers alone showed this elongation (Figures S2C and S2D). The experimental assemblies exhibited robust asymmetric patterning, with 92% showing distinct SOX2/TBXT expression domains. TBXT expression localized specifically near GFP-signaling centers, while controls maintained uniform OCT4/SOX2 distribution (Figures 1J, 1K, and S2E). Further analysis showed that the GFP-proximal region expressed CDX2 and HOXB9 (tailbud markers in mammalian embryos)[54,55], indicative of posterior identity. At the opposite pole, we detected expression of the anterior markers OTX2 and LHX5[56], located away from the GFP-signaling center (Figures 1L, S10A, and S10B). These spatially restricted responses suggest that the localized signaling center provides positional cues associated with the establishment of anterior-posterior polarity and axial elongation.

Evaluation of gastrulation

To assess the progression of gastrulation, qPCR analysis revealed significant upregulation of *TBXT* and *MIXL1* in hPSC aggregates assembled with signaling centers compared with isolated controls, supporting the induction of gastrulation-associated programs in the assembly models (Figure S2F). IF analysis identified a primitive streak (PS)-specific marker TBXT-positive domain adjacent to the GFP-signaling center (Figure 2A). The PS identity was further supported by co-expression of TBXT/MIXL1 and TBXT/EOMES, characteristic molecular signatures of the primitive streak[57,58] (Figure 2B). Based on these findings, we designated the assembled structures as “gastruloids.” In the natural gastrula, posterior epiblast cells within the PS undergo delamination and inward migration[59]. In our model, TBXT-positive cells showed the onset of N-cadherin (N-CAD) expression, suggestive of epithelial-to-mesenchymal transition (EMT)-associated changes. This was accompanied by a clear spatial divergence between N-CAD and E-cadherin (E-CAD) expression patterns in the epiblast region, providing additional evidence for delamination near the signaling hub (Figure 2C). Live-cell imaging captured GFP-proximal cells moving inward from the gastruloid surface, providing additional evidence for this dynamic process (Figure S4A and Video S2). Interestingly, assemblies containing dual signaling centers developed two distinct TBXT-positive domains (Figure S4B), suggesting that the position of the signaling center influences the site of gastrulation initiation.

The emergence of SOX17-positive cells adjacent to the PS-like structure suggested endodermal specification[60] (Figure 2A). Molecular characterization confirmed the presence of cells co-expressing SOX17/GATA6 and

Langtaosha (LTS) Preprint doi: https://doi.org/10.65215/LTSpreprints.2026.08.25.000317. This version posted August 26, 2026. The copyright holder for this preprint (which was not certified by peer review) is the author/funder. Creative Commons license: CC Attribution-NonCommercial-NoDerivatives 4.0 https://creativecommons.org/licenses/by-nc-nd/4.0

SOX17/FOXA2 (Figures 2D and S4C), canonical markers of developing endoderm. Notably, SOX17/GATA6 double-positive cells exhibited a spatially organized distribution within gastruloids, suggesting regionalized endodermal patterning (Figure 2D). Further analysis revealed the presence of SOX17/SOX9 double-positive progenitors (Figure S4D), suggesting an endodermal population with features associated with intestinal development[61]. The absence of these gastrulation-related phenotypes in control aggregates confirmed that spontaneous gastrulation did not occur in basal medium (Figure S2E-S2H), supporting a requirement for signaling center-derived cues in initiation of these gastrulation-like events.

In summary, day 5 gastruloids capture key aspects of early human development, including anterior-posterior symmetry breaking and axial elongation, PS-like features, and germ layer specification. The protocol demonstrated consistent reproducibility across multiple hPSC lines (H9 and RUES2) (Figure S5), supporting its robustness across different hPSC backgrounds.

Single-cell transcriptomic characterization of gastruloids

To comprehensively characterize the cellular composition of our model, we performed single-cell RNA sequencing (scRNA-seq) on approximately 50 pooled day 5 gastruloids from each of two independent experiments. After stringent QC filtering (500 < genes < 7000, 1000 < RNAs < 40000, and mitochondrial reads < 25%) and doublet removal, 5158 high-quality single-cell transcriptomes were retained for downstream analysis.

Uniform Manifold Approximation and Projection (UMAP) analysis revealed 12 major cell clusters (Figures 3A-3C), which were annotated based on established lineage-specific markers and comparisons with previous single-cell studies of human and non-human primate gastrulating embryos[44,45,62-65]. Importantly, the two biological replicates showed highly similar cluster distributions (Figures 3A and S7A), supporting the reproducibility of the cellular composition generated by our model.

We first identified an epiblast-like cluster (EPI) expressing the genes *DNMT3B*, *UTF1*, and *TDGF1*, along with pluripotency markers *POU5F1* (OCT4), *NANOG*, and *SOX2* (Figures 3C, S6A, and S6B). Adjacent to this population, neural ectoderm (NE) cells expressed neural markers *SOX2*, *PAX6*, *SOX3*, *HESX1*, *SIX3*, and *OTX2* (Figures 3C, S6B, and S6C). We also found an anterior neural ectoderm (ANE) population expressing these neural markers along with anterior neural transcription factors *FOXG1*, *EMX2*, *LHX5*, *LHX2*, *OTX1*, and *OTX2* (Figures 3C and S6C), which are established regulators of

Langtaosha (LTS) Preprint doi: https://doi.org/10.65215/LTSpreprints.2026.08.25.000317. This version posted August 26, 2026. The copyright holder for this preprint (which was not certified by peer review) is the author/funder. Creative Commons license: CC Attribution-NonCommercial-NoDerivatives 4.0 https://creativecommons.org/licenses/by-nc-nd/4.0

brain development[56,66-69]. Within the non-neural ectoderm (NNE) population, which expressed *TFAP2A*, *TFAP2C*, and *DLX5*, neural crest (NC) cells were further distinguished by markers including *PAX3*, *PAX7*, *SOX10*, *SOX9*, and *FOXD3* (Figures 3C, S6D, and S6E).

In mesendodermal lineages, a PS population expressed gastrulation-associated markers *TBXT*, *MIXL1*, and *EOMES* (Figures 3C and S6F). Nascent mesoderm (NM) cells, marked by *TBX6*, *MESP1*, *MSGN1*, *RSPO3*, and *FOXC1*, retained expression of PS markers *TBXT*, *MIXL1*, and *EOMES*, consistent with an early mesodermal state emerging from the PS (Figures 3C, S6F, S6G, and S11C). As mesodermal populations progressed toward more differentiated states, emergent mesoderm (EM) displayed decreased *TBXT* and elevated expression of other mesodermal markers such as *LHX1*, *IRX3*, and *PDGFRA* (Figures 3C and S6H). Advanced mesoderm (ADM) exhibited decreased *TBX6*/*MESP1* and high levels of *FOXF1*, *HAND1*, *HAND2*, *GATA4*, *GATA6*, *NKX2*.5, *MYL7*, and *ACTC1* (Figures 3C, S6I, S6K, and S6M). The juxtaposition and divergence of TBXT, LHX1, TBX6, FOXF1, HAND1, and HAND2 reflected the dynamic process of mesodermal development (Figures S4E-S4G and S6F-S6I). A distal mesoderm cluster that lacked the embryonic marker (*TBXT*) but expressed extraembryonic mesenchyme-associated transcription factors, including *FOXF1* and *HAND1*, together with markers such as *ANXA1*, *POSTN*, *LUM*, and *NID2*, was annotated as an extraembryonic mesenchyme-like population (EXM)[44,45,62,70-72] (Figures 3C, S6F, S6I, and S6J). IF analyses confirmed the expression of EXM-associated markers HAND1, LUM, POSTN, and ANXA1 in gastruloid tails (Figures S4H and S4I). We also identified an endoderm (END) population marked by *SOX17*, *FOXA2*, *CST1*, *GATA6*, and *GATA4* (Figures 3C and S6K). Notably, the enrichment of *PECAM1* (CD31), *MEF2C*, *CDH5*, and *CD34* identified a population with endothelial progenitor (EP)-like features (Figures 3C and S6L). Together, these findings demonstrate that the model reproducibly generates a diverse cellular landscape spanning pluripotent, germ-layer, and early organ-associated states.

Comparisons with reported single-cell datasets

To validate the physiological relevance of our gastruloids, we performed systematic comparisons with single-cell transcriptomic datasets from Carnegie Stage (CS) 7-8 human embryos[44,45]. Integrated analysis demonstrated strong concordance between our day 5 gastruloids and natural human gastrulae, with recapitulation of major lineages: epiblast, primitive streak, ectodermal derivatives, mesodermal subtypes, endoderm, endothelial progenitors, and extraembryonic mesenchyme (Figure 3D). Notably, similarity analysis

Langtaosha (LTS) Preprint doi: https://doi.org/10.65215/LTSpreprints.2026.08.25.000317. This version posted August 26, 2026. The copyright holder for this preprint (which was not certified by peer review) is the author/funder. Creative Commons license: CC Attribution-NonCommercial-NoDerivatives 4.0 https://creativecommons.org/licenses/by-nc-nd/4.0

comparing our gastruloids with natural CS7-8 human gastrulae data corroborated both our lineage annotations and the model's ability to capture the germ layer diversity of gastrulation-stage embryos (Figures 3E and 3F).

Cross-species comparisons revealed conserved transcriptional features between our gastruloids and cynomolgus monkey gastrulae (CS8) and mouse embryos (E6.5-E7.25)[62,73], further supporting the developmental relevance of our model (Figures S7B-S7E). When benchmarked against existing human embryo models, including the peri-gastruloid[18] and synthetic embryos model (SEM)[15], our model demonstrated accessibility in covering gastrulation-associated lineages (Figure S8). Together, these comparisons support the developmental relevance of our model, showing that its cellular states capture key transcriptional features of human gastrulation as well as conserved programs shared across species.

Spatial organization of BMP signaling in gastruloids

Cell-cell communication analysis revealed a prominent BMP signaling network in gastruloids, including predicted BMP2/4 ligand-receptor interactions (Figures S9A-S9C). Spatial transcriptome analysis further supported the anterior-posterior polarization and revealed a spatially organized BMP signaling landscape, with GFP-positive regions showing enriched expression of *BMP2* and *BMP4* (Figures S9D-S9F). Consistent with these transcriptional patterns, IF detected BMP2/4 proteins in close proximity to GFP-positive cells, together with nuclear accumulation of phosphorylated SMAD1/5/9, indicative of active BMP signal transduction[74] (Figures S9G). Functional perturbation with the BMP pathway inhibitor LDN193189[75] (LDN) strongly disrupted axial elongation and abolished mesodermal differentiation (Figures S9H-S9J). Collectively, these results identify BMP signaling as a spatially organized signaling component associated with gastruloid patterning and provide functional evidence for its contribution to axial elongation and mesodermal differentiation[76-78].

Neural development in gastruloids

Single-cell transcriptomics identified three distinct neural lineages in our gastruloids: neural ectoderm (NE) expressing *SOX2*, *PAX6*, *SOX3*, *HESX1*, *SIX3*, and *OTX2*; anterior neural ectoderm (ANE) enriched for brain regulators *FOXG1*, *EMX2*, *LHX5*, *LHX2*, *OTX1*, and *OTX2*; and neural crest (NC) marked by *PAX3*, *PAX7*, *SOX10*, *SOX9*, and *FOXD3* (Figures 3B, 3C, and S6B-S6D). Notably, neural progenitors identified in our gastruloids were not observed in reference CS7-8 human embryos (Figure 3D), suggesting that the model extends beyond this developmental window and captures early neural

Langtaosha (LTS) Preprint doi: https://doi.org/10.65215/LTSpreprints.2026.08.25.000317. This version posted August 26, 2026. The copyright holder for this preprint (which was not certified by peer review) is the author/funder. Creative Commons license: CC Attribution-NonCommercial-NoDerivatives 4.0 https://creativecommons.org/licenses/by-nc-nd/4.0

specification events associated with later developmental stages[44,45].

To validate neural developmental progression in our model, we performed a comparative analysis with a CS10 (PCW3) human embryo dataset[47], focusing on corresponding neural cell types, such as neural tube populations (NT 1-3) and neural crest (Figure 4A). Transcriptomic alignment revealed similarity between gastruloid-derived neural populations and their *in vivo* counterparts at this later developmental stage (Figure 4B), supporting the presence of early neural developmental features beyond gastrulation. Morphological and molecular characterization revealed hallmarks associated with neural morphogenesis, including the emergence of a neural groove-like structure, the presence of SOX3/PAX6/SOX2 triple-positive neural tissues, and a pseudostratified-like neuroepithelium, as demonstrated by PAX6/Phalloidin co-staining (Figures 4C-4G). The co-existence of folding and closed neural plate regions within the same gastruloid captured the dynamic neural morphogenetic process in our model (Figures 4F and 4G). SOX10-positive NC populations exhibited dorsal enrichment consistent with the *in vivo* distribution, while a small fraction of ventral NC cells suggested migratory behavior (Figure 4G). Anterior neural specification was further supported by the presence of LHX5/PAX6 double-positive neural progenitors and cells co-expressing key forebrain transcription factors such as LHX5/FOXG1, OTX2/SIX3, and LHX5/OTX2 (Figures 4H, 4I, S10A, and S10B)[56,66-68]. These neural developmental features were reproducibly observed across multiple gastruloids, with SOX1/SOX2/ZO1 triple-positive neural tissues and an OTX2-positive anterior region containing SOX10-positive cells further supporting regionalized neural specification (Figure S10C).

During secondary neurulation, neuromesodermal progenitors (NMPs)—transient bipotent cells at the caudal end—coordinate axial elongation through balanced self-renewal and differentiation[79]. SOX2/TBXT double-positive cells were detected in the GFP-proximal posterior region of gastruloids (Figure S11A). At single-cell resolution, *SOX2*/*TBXT* double-positive cells expressed NMP-associated transcription factors (*NKX1-2*, *CDX1*, *CDX2*, *SP5*, and *SP8*), signaling ligands (*WNT3A*, *WNT5B*, *WNT8A*, *FGF4*, and *FGF17*), and retinoic acid (RA)-related regulators (*ALDH1A2* and *CYP26A1*)[47,65,79-83]. These NMP-like populations occupied an intermediate position between neuroectoderm and an adjacent population expressing paraxial mesodermal markers (*MSGN1*, *TBX6*, *MESP1*, and *RSPO3*) (Figures S11B and S11C). Collectively, these findings suggest that the signaling center is associated with the emergence of a transient progenitor state that may provide continuity between neural and

Langtaosha (LTS) Preprint doi: https://doi.org/10.65215/LTSpreprints.2026.08.25.000317. This version posted August 26, 2026. The copyright holder for this preprint (which was not certified by peer review) is the author/funder. Creative Commons license: CC Attribution-NonCommercial-NoDerivatives 4.0 https://creativecommons.org/licenses/by-nc-nd/4.0

mesodermal developmental programs during axial extension[79].

Spatial neural patterning involves coordinated regulation of the SHH pathway and antagonistic BMP signaling[84-87]. scRNA-seq identified *SHH*-positive cells co-expressing BMP antagonists (*NOGGIN* and *CHRD*) and key transcription factors *FOXA2* and *FOXA1*. These cells partially overlapped with *GFP mRNA*-positive descendants, suggesting their association with the signaling center (Figures S12A and S12B). IF analysis further confirmed that GFP-descendant FOXA2-positive cells expressed both SHH and NOGGIN (Figure S12C). These factors constitute a signaling network with established roles in embryonic axis patterning and early neural development[88-91], suggesting that signaling center-derived cells establish a localized SHH–BMP antagonistic signaling environment associated with the spatial specification of neural tissues.

Extended-cultured gastruloids exhibit cardiac- and endothelial-associated structures

The heart, as the first functional organ to emerge, serves as a hallmark of early organogenesis occurring during CS10-11[92]. Single-cell analysis revealed cardiogenic precursor specification through the expression of core regulators, including transcription factors (*GATA4*, *GATA6*, and *NKX2.5*), structural components (*MYL7* and *ACTC1*), and the signaling receptor *KDR*[93,94] (Figures S6K and S6M). To assess their developmental potential, we extended the culture in basal medium and observed spontaneous rhythmic contractions in anterior regions of gastruloids from day 9 onward (Figures 5A, 5B, S13A, and Videos S3-S5). This phenotype was observed at an average frequency of 22.5% across multiple independent experiments (Figure 5C). We named these beating gastruloids “PANPANs”, inspired by the “pan-pan” sound that we associated with their spontaneous heartbeat-like activity, and numbered them sequentially based on the order of discovery. The beating cardiac-like domain in PANPAN exhibited features associated with heart development, including expression of cardiac muscle troponin T (cTnT) and transcription factors *GATA4*/*6*, and *MEF2C*[93,94] (Figures 5D and 5E). Immunostaining of multiple PANPANs consistently revealed a similar cardiac cavity localized within the anterior region (Figures S13B-S13D). Consistent with the involvement of intracellular calcium (Ca^{2+}) dynamics in cardiomyocyte contraction[94-96], the PANPAN cardiac-like domains exhibited synchronized calcium transients during spontaneous beating (Figures 5F-5H, and Video S6).

We next assessed endothelial-associated features in PANPANs following the emergence of cardiac-like domains. At the single-cell level, cells displaying

Langtaosha (LTS) Preprint doi: https://doi.org/10.65215/LTSpreprints.2026.08.25.000317. This version posted August 26, 2026. The copyright holder for this preprint (which was not certified by peer review) is the author/funder. Creative Commons license: CC Attribution-NonCommercial-NoDerivatives 4.0 https://creativecommons.org/licenses/by-nc-nd/4.0

endothelial-associated profiles expressed key markers, including *PECAM1* (CD31), *MEF2C*, *CDH5*, and *CD34*[44,45,62] (Figure S6L). Outside the cardiac-like domain, MEF2C expression was also observed in adjacent regions, prompting further assessment of endothelial-associated features given its established role in cardiac and vascular development[97] (Figures 5D, and S13B-S13D). In parallel, immunostaining for CD31 and CD34 revealed an extensive endothelial-like network of spindle-shaped cells distributed throughout PANPANs[98,99] (Figures 5I, 5J, and S13E). Additionally, we observed CD31-positive endothelial-associated structures containing internal spaces, indicative of early lumen-like features (Figure S13F).

Expression of FOXG1, a key regulator of brain development[66], adjacent to the cardiac domains suggested coordinated neuro-cardiac patterning (Figure S14A). SHH expression in GFP-positive descendants was observed along the midline of PANPAN, consistent with the spatial distribution of a signaling factor implicated in neural and axial patterning (Figure S14A)[85,86,88]. Ventrally, SOX17-positive cells displayed an epithelial organization marked by E-CAD expression[94] (Figures S14B and S14C). The emergence of anterior SOX2/SOX17/E-CAD and posterior SOX17/HOXB9/CDX2 triple-positive cells suggested regionalized endodermal patterning, with the posterior populations exhibiting features associated with hindgut development[100,101] (Figures S14D and S14E). These findings reveal spatially patterned features across multiple tissue domains during early organogenic development.

To more comprehensively characterize the cell types within PANPANs, we performed scRNA-seq on the beating gastruloids. Single-cell analyses further confirmed that our model reproducibly gives rise to a spectrum of early organ-associated lineages, including neural, cardiac, and vascular populations (Figures S15A and S15B). Furthermore, by benchmarking these single-cell transcriptomic profiles against published *in vivo* transcriptomic datasets from human CS10 and CS12 embryos[46,47] (Figures S15C-S15E), we placed the observed developmental features within the context of human early organogenesis. Notably, no additional lineage-specific induction factors were introduced throughout the culture period; instead, development proceeded following the assembly of the WNT/NODAL-induced signaling center. These findings suggest that spatial signaling asymmetry provides an organizing framework linking gastrulation-associated patterning to the coordinated emergence of early organogenic programs.

Comparative analysis of distinct signaling centers in assembled models

Using this assembled gastruloid system, we examined how signaling

Langtaosha (LTS) Preprint doi: https://doi.org/10.65215/LTSpreprints.2026.08.25.000317. This version posted August 26, 2026. The copyright holder for this preprint (which was not certified by peer review) is the author/funder. Creative Commons license: CC Attribution-NonCommercial-NoDerivatives 4.0 https://creativecommons.org/licenses/by-nc-nd/4.0

centers generated by distinct pathway inputs influence the developmental behavior of the assembled structures. We established signaling centers activated by BMP4, WNT (CHIR)[49], NODAL (Activin A)[50], or combined WNT/NODAL signaling (Figure S16). Each signaling center was paired with untreated hPSC aggregates using the same assembly configuration, enabling direct comparison of their integration and developmental outcomes (Figure S17).

WNT/NODAL co-activated centers consistently established stable polarity relative to untreated aggregates. In contrast, BMP4- or WNT-only centers readily fused with the aggregates within 24 hours, while NODAL-only centers exhibited an intermediate phenotype (Figures S17A-S17G). Notably, robust axial elongation was observed only in gastruloids containing WNT/NODAL co-activated hubs (Figures S17A-S17L). Although BMP4- and Activin A-only conditions induced mesendodermal markers, including TBXT and SOX17 (Figures S17M-S17O), these responses were not accompanied by axial elongation (Figures S17B-17L). These results indicate that mesendoderm induction alone is insufficient to establish the polarized, elongating architecture of the gastruloid, and point to a specific requirement for coordinated WNT/NODAL activity in establishing a signaling center capable of supporting axial organization[37,48].

Bulk transcriptomic analyses further showed that WNT/NODAL co-activated centers exhibit a distinct transcriptional signature, characterized by elevated expression of secreted ligands and cell adhesion-related genes (Figure S18). The enrichment of these gene programs is consistent with a signaling state characterized by increased capacity for intercellular communication and cell-cell interactions, which may help sustain the spatial organization of the assembled gastruloid.

Discussion

Early organ primordium formation unfolds through a progressive sequence of cell fate transitions and morphogenetic changes initiated during gastrulation. Capturing this window *ex vivo* remains a major challenge in developmental and stem cell biology. Existing human and non-human primate systems, including gastruloids, post-implantation models, and *ex vivo* cultures of early primate embryos, often reach a developmental plateau prior to coordinated organogenesis[18-20,63,64,102-106], highlighting the challenge of sustaining developmental progression beyond gastrulation. In this study, we show that introducing a localized signaling center enables the transition from human

Langtaosha (LTS) Preprint doi: https://doi.org/10.65215/LTSpreprints.2026.08.25.000317. This version posted August 26, 2026. The copyright holder for this preprint (which was not certified by peer review) is the author/funder. Creative Commons license: CC Attribution-NonCommercial-NoDerivatives 4.0 https://creativecommons.org/licenses/by-nc-nd/4.0

gastrulation-associated patterning toward early organogenic development. By establishing an organizer-inspired signaling center through transient co-activation of the WNT and NODAL pathways, we engineered a minimal hPSC assembly capable of autonomous symmetry breaking, robust axial elongation, germ layer organization, and the progressive specification of spatially distinct neural, cardiac, and endothelial tissues.

While some human models have demonstrated remarkable success in generating organotypic structures, they often employ the sequential application of global exogenous growth factors to guide differentiation[23-33]. Such approaches may place greater emphasis on externally imposed differentiation cues than on the reciprocal interactions between tissue organization and endogenous signaling. In contrast, our system is organized around a spatially localized center that initiates and sustains the developmental program. By enabling transitions from gastrulation to organogenic development without complex protocol switching, our findings highlight the intrinsic self-organizing capacity of hPSC. Once the initial axis is established by a localized center, subsequent lineage emergence and tissue patterning can proceed with limited additional external input. Our study therefore suggests that the key to linking gastrulation with early organogenesis is not simply the sequential induction of additional cell fates, but the establishment of spatially asymmetric signaling that allows multiple developmental programs to emerge in a coordinated manner. Consequently, the core innovation here is not simply extending differentiation to later developmental endpoints, but introducing organizer-inspired spatial signaling to investigate how spatially restricted cues shape human development[48,51]. Nevertheless, we acknowledge that this model does not fully recapitulate all aspects of organogenesis, including organized somitogenesis, which may require additional developmental cues and tissue interactions beyond the current minimal system.

Although signaling center-guided strategies have been applied in mouse embryo models, translating this approach to human systems poses species-specific challenges. hPSCs exhibit distinct biological properties and developmental competencies compared to their murine counterparts[107,108]. Moreover, human embryogenesis unfolds over an extended developmental timeline and requires precise spatiotemporal coordination among germ layers, which further complicates *in vitro* modeling efforts[59,60]. Our implementation demonstrates that, despite these complexities, a minimalist signaling logic—specifically, coordinated activation of WNT and NODAL—can initiate and support axial patterning, germ layer organization, and early organogenic

Langtaosha (LTS) Preprint doi: https://doi.org/10.65215/LTSpreprints.2026.08.25.000317. This version posted August 26, 2026. The copyright holder for this preprint (which was not certified by peer review) is the author/funder. Creative Commons license: CC Attribution-NonCommercial-NoDerivatives 4.0 https://creativecommons.org/licenses/by-nc-nd/4.0

development in a human context.

A key strength of this platform is that both the signaling center and the responding tissues are derived from humans, enabling interrogation of signaling center function within a fully human-derived cellular context. Maintaining both components within a species-matched system circumvents the ethical and practical constraints associated with *in vivo* allogeneic transplantation in humans and avoids the interspecies variability inherent in xenogeneic transplantation assays[36,37,48,51]. This species-matched platform may therefore provide an opportunity to examine whether organizer activities inferred from xenotransplantation studies are conserved and functionally relevant within a human developmental context[48,51]. We note that the developmental behavior of this signaling center may not fully recapitulate the classical organizer activity defined in transplantation assays. The neighboring cells instead exhibit gastrulation-related features reminiscent of those observed following transplantation of primitive streak-associated regions in avian embryos[109]. However, due to the limited accessibility of human embryos for functional testing, the *in vivo* properties of human signaling centers remain incompletely defined, underscoring the importance of this model for exploring their roles in developmental patterning.

Our approach is based on a minimalist strategy that leverages the intrinsic self-organizing capacity of hPSCs while avoiding the need for extensive external manipulation or complex engineering platforms, such as microdevices or optogenetic systems[38-41]. We propose that this concept could be expanded by incorporating additional signaling centers associated with extraembryonic populations, such as the trophoblast, amnion, hypoblast, and anterior visceral endoderm[12,15,18,110-112], to initiate distinct and autonomous developmental programs. Although our current model acquires features associated with early organogenesis following gastrulation, it does not yet incorporate extraembryonic morphogenesis (e.g., amniotic cavity or yolk sac formation). Future integration of organizer-like centers with extraembryonic elements may enable the development of more comprehensive embryo-like systems. From this perspective, the significance of our findings extends beyond the assembled gastruloid system itself: organizer-like cells generated here could, in principle, be integrated into existing human embryo-like models to potentially enhance developmental competence and support more sustained developmental progression.

Efficient nutrient exchange and waste removal become increasingly important as developing organisms increase in size and complexity, as diffusion

Langtaosha (LTS) Preprint doi: https://doi.org/10.65215/LTSpreprints.2026.08.25.000317. This version posted August 26, 2026. The copyright holder for this preprint (which was not certified by peer review) is the author/funder. Creative Commons license: CC Attribution-NonCommercial-NoDerivatives 4.0 https://creativecommons.org/licenses/by-nc-nd/4.0

alone is insufficient to support larger structures such as embryos, necessitating the gradual establishment of circulatory systems[92]. This transport challenge also represents a major limitation for long-term organoid culture[113]. The spontaneous emergence of cardiac- and endothelial-like tissues in our model provides an opportunity to investigate how early cardiovascular features may support extended developmental progression. Human embryonic circulation develops gradually through complex yet incompletely understood processes, owing in part to ethical and technical barriers limiting direct investigation of early embryonic cardiovascular development[92,93]. Even in extended *ex vivo* cynomolgus cultures, key milestones like the onset of a heartbeat remain difficult to capture[63,64]. These limitations highlight the value of our stem cell-based model as an accessible platform for investigating early human cardiogenesis and vascular development. Despite the emergence of early cardiac-like activity, physiological circulation has not yet been established in our model. This limitation may be related to the absence of yolk sac-associated extraembryonic structures, which are essential for early hematopoiesis[114]. As previously discussed, integrating additional extraembryonic components may be important for supporting further cardiovascular maturation and vascular development.

In summary, our findings highlight signaling asymmetry as a fundamental organizing principle of human development, whereby a localized signaling center provides spatial information that coordinates lineage allocation and supports progression from gastrulation to early organogenesis. Rather than independently inducing neural, cardiac, or endothelial fates, the signaling center establishes a spatially asymmetric environment in which these programs emerge in coordinated positions and developmental sequence. Beyond developmental biology, our platform may inform future strategies for generating developmentally relevant human tissues in regenerative medicine.

Limitations of the study

There are several limitations in our model. (1) The absence of extraembryonic tissues, including trophoblast, amnion, and yolk sac lineages, limits the incorporation of extraembryonic interactions that contribute to human embryonic development. Future integration of organizer-like centers with additional extraembryonic components may enable more comprehensive embryo-like models. However, efforts toward increasingly complete stem cell-based embryo models should be accompanied by careful consideration of emerging ethical implications, particularly regarding their potential similarity to

Langtaosha (LTS) Preprint doi: https://doi.org/10.65215/LTSpreprints.2026.08.25.000317. This version posted August 26, 2026. The copyright holder for this preprint (which was not certified by peer review) is the author/funder. Creative Commons license: CC Attribution-NonCommercial-NoDerivatives 4.0 https://creativecommons.org/licenses/by-nc-nd/4.0

natural human embryos. (2) Optimization of culture platforms, such as dynamic culture systems (e.g., shaking or roller-based approaches), may provide improved conditions for prolonged development. (3) While minimizing exogenous signals highlights the intrinsic organizing potential of the signaling center, this strategy may limit long-term development and maturation due to a lack of the essential nutrients for sustained development. Adding factors like human cord blood serum might support the maturation and functional development of gastruloids.

RESOURCE AVAILABILITY

Materials availability

This study did not generate any unique reagents.

Data and code availability

scRNA-seq datasets in this study have been deposited in the NGDC database.

This paper does not report original code.

Any additional information required to reanalyze the data reported in this paper is available from the lead contact upon request.

ACKNOWLEDGMENTS

This work was supported by the National Key Research and Development Program of China (2022YFA1104100), the Shenzhen Medical Research Fund (A2403059), the National Key Research and Development Program of China (2024YFA1107900, 2021YFA1100603), the National Natural Science Foundation of China (32130046, 82471462 and 82270566), the Pioneering Talents Project of Guangzhou Development Zone (2021-L029), the China Postdoctoral Science Foundation (2025M771456), the Research Start-up Fund of Post-doctoral of SAHSYSU (ZSQYRSFPD0083), and the Shenzhen Science and Technology Innovation Commission (QNXMC20250701093516022).

AUTHOR CONTRIBUTIONS

Conceptualization: W.L., A.P.X. and B.W.; Methodology: B.W., W.L., A.P.X., J.W., R.L., Dairui L. and L.C.; Investigation: B.W., H.Y., R.L., Junhua C., W.Y., X.W., Dairui L., H.L., Jierui C., Y.W., S.H., L.W., Z.L., C.W., J.D., Q.C., T.W., Z.T.,

Langtaosha (LTS) Preprint doi: https://doi.org/10.65215/LTSpreprints.2026.08.25.000317. This version posted August 26, 2026. The copyright holder for this preprint (which was not certified by peer review) is the author/funder. Creative Commons license: CC Attribution-NonCommercial-NoDerivatives 4.0 https://creativecommons.org/licenses/by-nc-nd/4.0

Dongjun L., and Bruce T. Lahn; Visualization: B.W., H.Y., R.L., Junhua C., and W.Y.; Funding acquisition: A.P.X., W.L., L.C., and B.W.; Supervision: A.P.X. and W.L.; Project administration: A.P.X. and T.W.; Writing – original draft: B.W., R.L, L.C., J.W., A.P.X. and W.L.; Writing – review & editing: B.W., R.L, L.C., J.W., A.P.X. and W.L.. All authors discussed and commented on the manuscript.

DECLARATION OF INTERESTS

The authors declare no competing interests.

Langtaosha (LTS) Preprint doi: https://doi.org/10.65215/LTSpreprints.2026.08.25.000317. This version posted August 26, 2026. The copyright holder for this preprint (which was not certified by peer review) is the author/funder. Creative Commons license: CC Attribution-NonCommercial-NoDerivatives 4.0 https://creativecommons.org/licenses/by-nc-nd/4.0

Figure 1. Construction of a signaling center-guided model

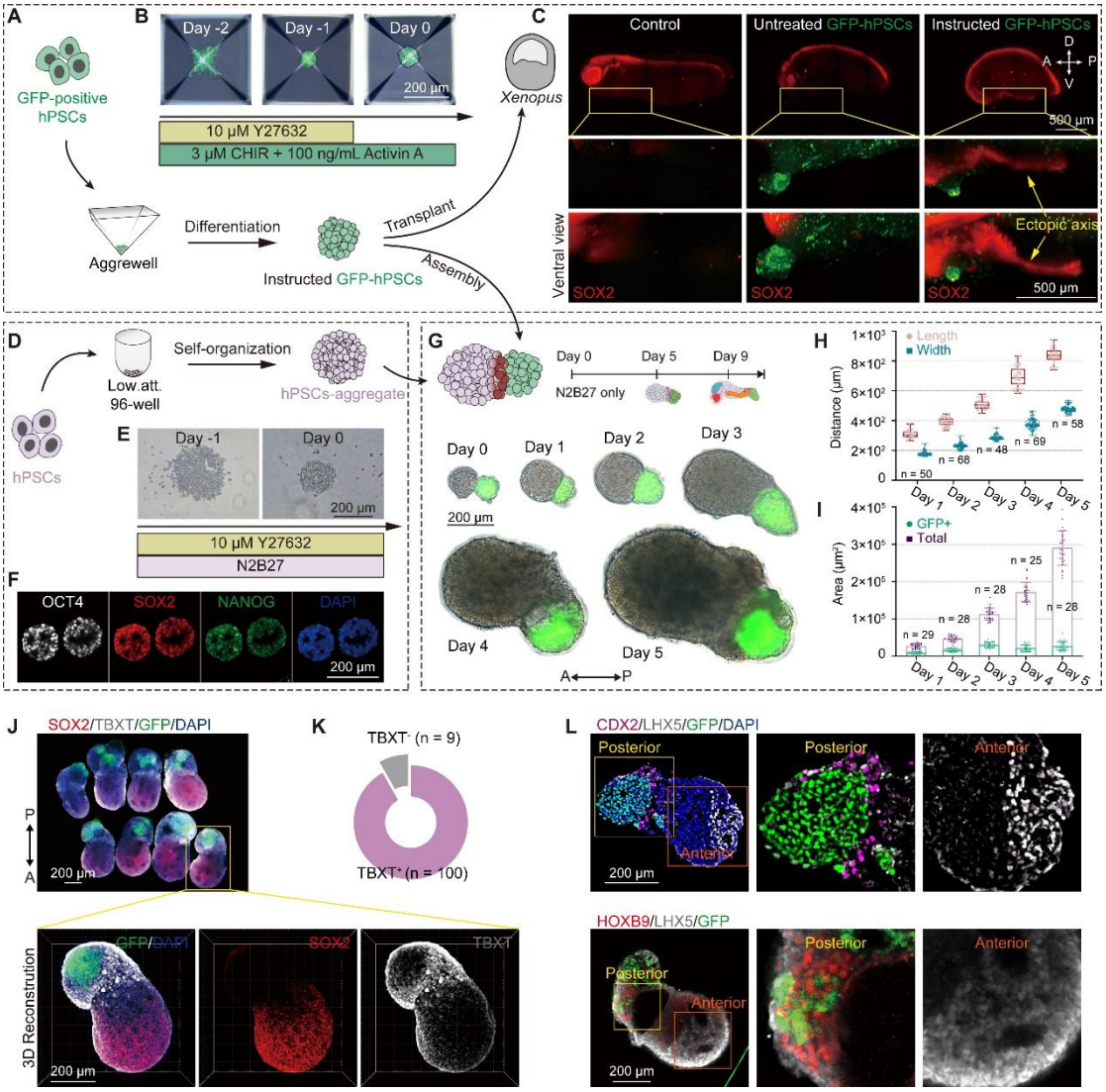

(A) Schematic illustrating the induction of a signaling center from GFP-positive human pluripotent stem cells (GFP-hPSC).

(B) Top, time-course development of instructed GFP-hPSC; bottom, schematic of the culture protocol. CHIR, CHIR99021.

(C) IF image showing SOX2-positive neural tissues in control *Xenopus* embryo or those transplanted with untreated or instructed GFP-hPSC. A: anterior; P: posterior; D: dorsal; V: ventral.

(D) Schematic illustrating GFP-negative hPSC aggregate formation.

(E) Top, time-course formation of hPSC aggregate; bottom, schematic of the culture protocol.

(F) IF showing OCT4, SOX2 and NANOG expression in hPSC aggregates.

(G-I) Development of the assembly (gastruloid) of hPSC aggregate with a GFP-positive signaling center (G), and the corresponding measurement of length and width (H) and the area of GFP-positive and total regions (I) at different time points.

(J) IF showing SOX2 and TBXT expression in the gastruloids (top), and 3D

Langtaosha (LTS) Preprint doi: https://doi.org/10.65215/LTSpreprints.2026.08.25.000317. This version posted August 26, 2026. The copyright holder for this preprint (which was not certified by peer review) is the author/funder. Creative Commons license: CC Attribution-NonCommercial-NoDerivatives 4.0 https://creativecommons.org/licenses/by-nc-nd/4.0

635 reconstruction of a representative gastruloid (bottom).
636 (K) The proportion of gastruloids with GFP-negative cells expressing TBXT
637 (L) IF showing LHX5 and CDX2/HOXB9 expression in the gastruloids.
638

Langtaosha (LTS) Preprint doi: https://doi.org/10.65215/LTSpreprints.2026.08.25.000317. This version posted August 26, 2026. The copyright holder for this preprint (which was not certified by peer review) is the author/funder. Creative Commons license: CC Attribution-NonCommercial-NoDerivatives 4.0 https://creativecommons.org/licenses/by-nc-nd/4.0

Figure 2. Primitive streak-like feature and gastrulation

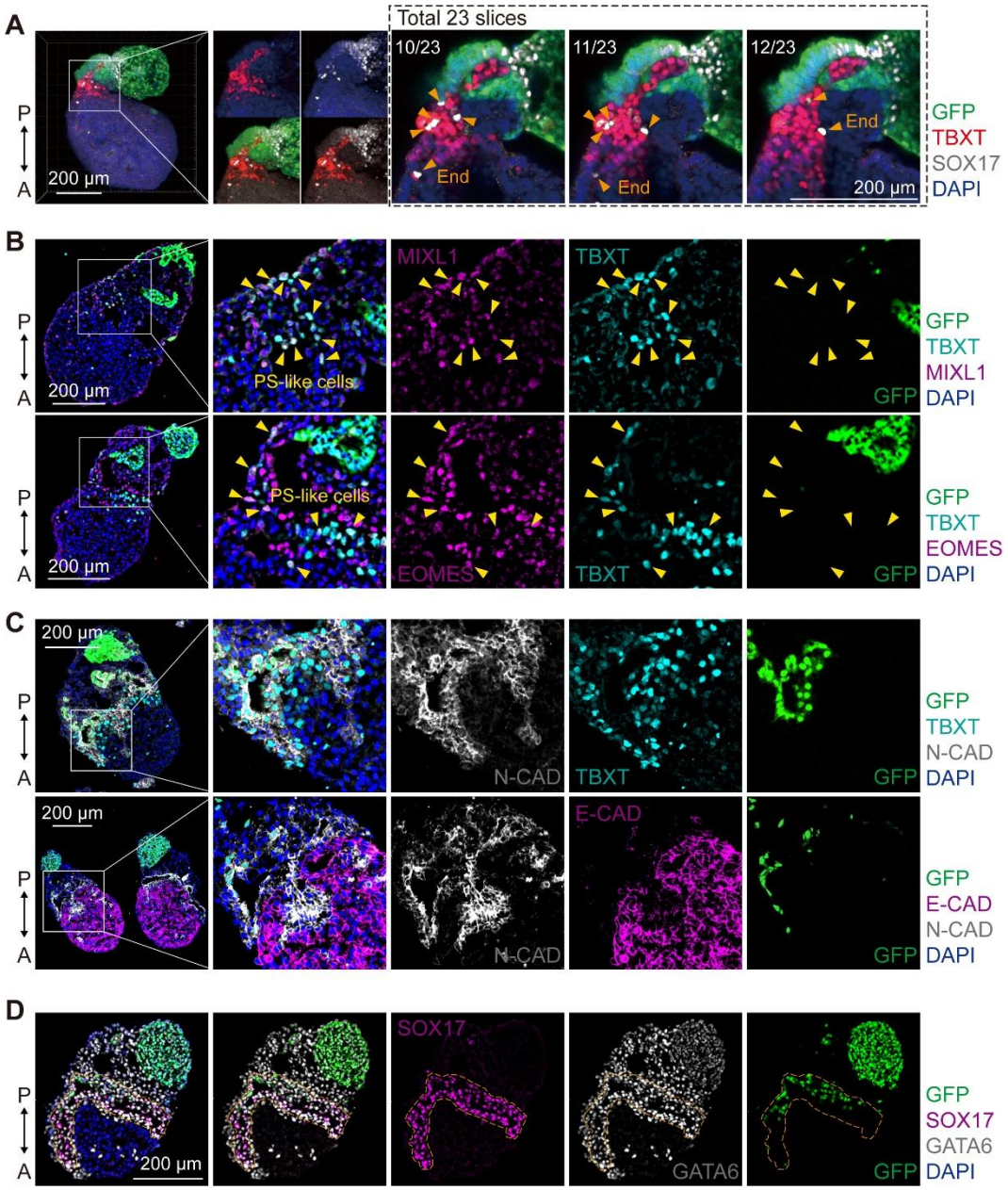

(A) Representative IF image of a day 5 gastruloid showing primitive streak (PS) and mesoderm specific marker TBXT-positive domain and SOX17-positive endodermal cells (End, orange triangle) are indicated. 3D reconstruction (left) and corresponding slices (right) are shown.
(B) Representative IF images of day 5 gastruloids. TBXT/MIXL1 (top) and TBXT/EOMES (bottom) mark the PS-like cells (yellow triangle).
(C) Representative IF images showing delaminating gastrulation cells (TBXT/N-CAD) and E-CAD-positive cells.
(D) Representative IF images showing endodermal cells (SOX17/GATA6).

Langtaosha (LTS) Preprint doi: https://doi.org/10.65215/LTSpreprints.2026.08.25.000317. This version posted August 26, 2026. The copyright holder for this preprint (which was not certified by peer review) is the author/funder. Creative Commons license: CC Attribution-NonCommercial-NoDerivatives 4.0 https://creativecommons.org/licenses/by-nc-nd/4.0

Figure 3. Single-cell RNA-seq analysis of gastruloids

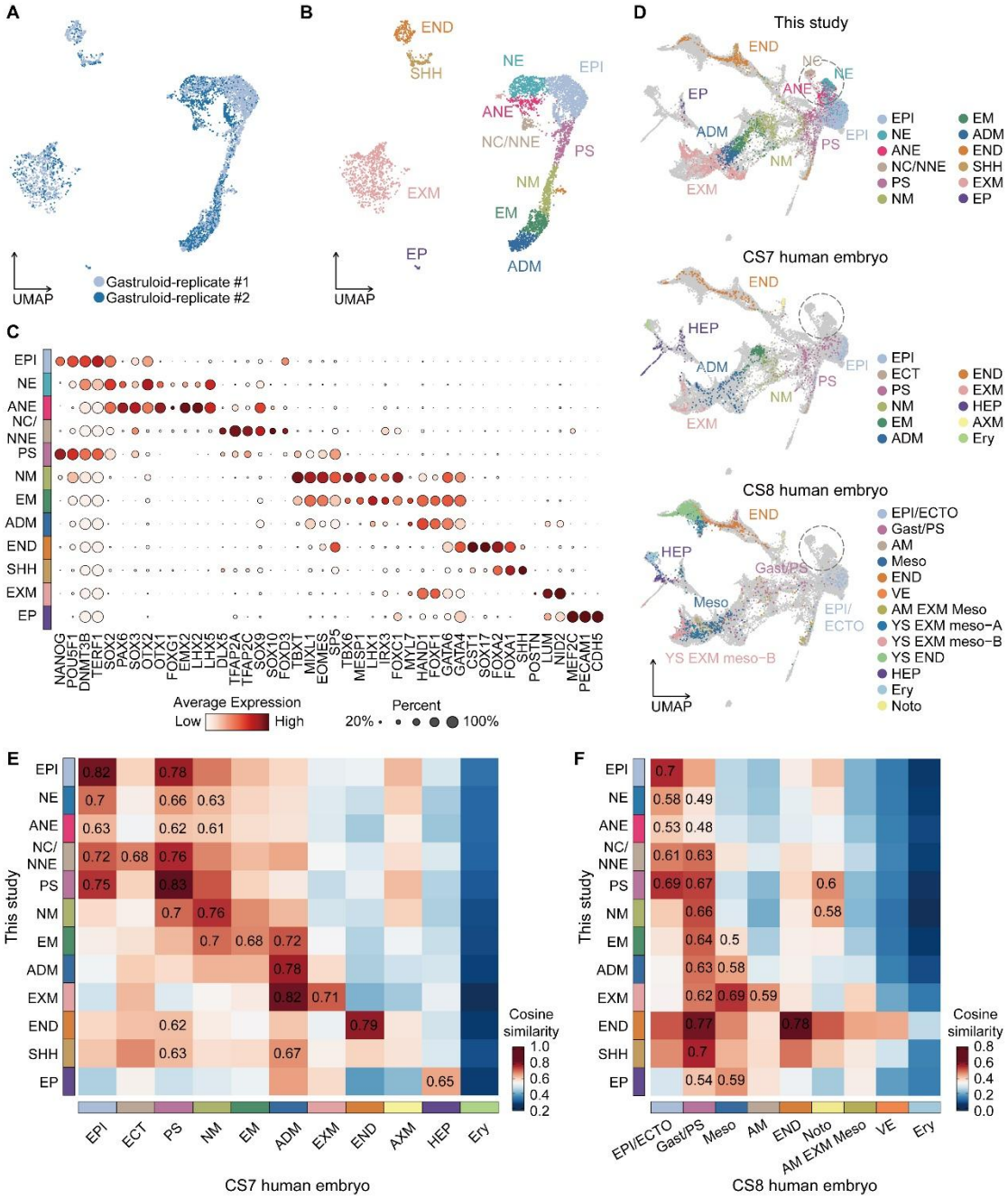

(A) Uniform Manifold Approximation and Projection (UMAP) visualization of individual cells from day 5 gastruloids across two independent experiments.
(B) UMAP plot showing twelve distinct colored clusters from (A), each representing different cell types: EPI, epiblast; NE, neural ectoderm; ANE, anterior neural ectoderm; NC, neural crest; NNE, non-neural ectoderm; PS, primitive streak; NM, nascent mesoderm; EM, emergent mesoderm; ADM, advanced mesoderm; EXM, extraembryonic mesenchyme; END, endoderm; EP, endothelial progenitors; SHH, SHH-positive cells.
(C) Dot plot showing average expression levels and proportion of cells expressing indicated genes in day 5 gastruloids clusters.
(D) UMAPs showing integration of day 5 gastruloids with reference human

Langtaosha (LTS) Preprint doi: https://doi.org/10.65215/LTSpreprints.2026.08.25.000317. This version posted August 26, 2026. The copyright holder for this preprint (which was not certified by peer review) is the author/funder. Creative Commons license: CC Attribution-NonCommercial-NoDerivatives 4.0 https://creativecommons.org/licenses/by-nc-nd/4.0

664 embryo cells. Top, gastruloids from this study; middle, CS7 human embryo;
665 bottom, CS8 human embryo. ECT, ectoderm; AXM, axial mesoderm; HEP,
666 haemato-endothelial progenitors; Ery, erythroblasts; EPI/ECTO,
667 epiblast/ectoderm; Gast/PS, gastrulating cell/primitive streak; AM, amnion;
668 Meso, mesoderm; VE, visceral endoderm; AM.EXE.Meso, amniotic extra-
669 embryonic mesoderm; YS.EXE.Meso-A/B, yolk sac extra-embryonic
670 mesoderm A/B; YS.END, yolk sac endoderm; Noto, notochord.
671 (E-F) Similarity heatmap comparing expression profiles of cell lineages
672 between gastruloids with CS7 (E) or CS8 (F) human embryos.
673

Langtaosha (LTS) Preprint doi: https://doi.org/10.65215/LTSpreprints.2026.08.25.000317. This version posted August 26, 2026. The copyright holder for this preprint (which was not certified by peer review) is the author/funder. Creative Commons license: CC Attribution-NonCommercial-NoDerivatives 4.0 https://creativecommons.org/licenses/by-nc-nd/4.0

Figure 4. Neural development in gastruloids

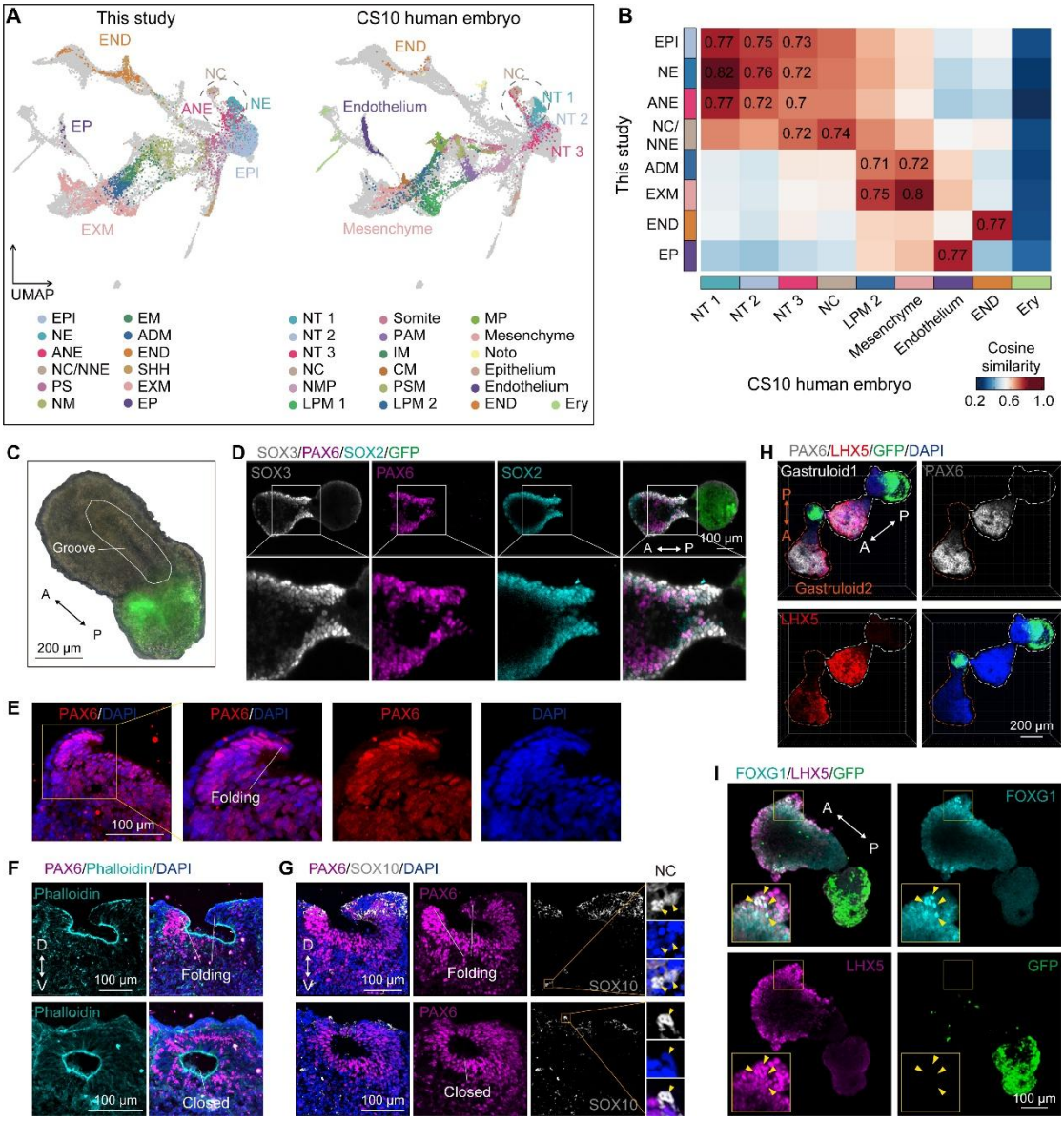

(A) UMAPs showing integration of day 5 gastruloids with CS10 human embryo cells. NT1/2/3, neural tube1/2/3; NC, neural crest; NMP, neuromesodermal progenitor; LPM1/2, lateral plate mesoderm1/2; PAM, paraxial mesoderm; IM, intermediate mesoderm; CM, cardiac myocyte; PSM, presomitic mesoderm; MP, myocyte progenitor; Noto, notochord; END, endoderm; Ery, erythroid.
(B) Similarity heatmap comparing expression profiles of cell lineages between gastruloids and CS10 human embryo.
(C) Representative merged fluorescence and brightfield images of a day 5 gastruloid. White lines outline a groove-like structure.
(D) Representative IF images of SOX3/PAX6/SOX2 triple-positive neural tissues.
(E) IF images showing folding neural plate stained for PAX6.
(F-G) IF images showing folding (top) and closed (bottom) neural plates stained with PAX6 and Phalloidin in different cryosections from the same gastruloid (F).

Langtaosha (LTS) Preprint doi: https://doi.org/10.65215/LTSpreprints.2026.08.25.000317. This version posted August 26, 2026. The copyright holder for this preprint (which was not certified by peer review) is the author/funder. Creative Commons license: CC Attribution-NonCommercial-NoDerivatives 4.0 https://creativecommons.org/licenses/by-nc-nd/4.0

690 Neural crest-like cells are stained for SOX10 (G).
691 (H) IF images showing expression of LHX5 and PAX6 in gastruloids.
692 (I) IF images showing expression of LHX5 and FOXG1 in gastruloids. Yellow
693 triangles indicate cells positive for both markers.
694

Langtaosha (LTS) Preprint doi: https://doi.org/10.65215/LTSpreprints.2026.08.25.000317. This version posted August 26, 2026. The copyright holder for this preprint (which was not certified by peer review) is the author/funder. Creative Commons license: CC Attribution-NonCommercial-NoDerivatives 4.0 https://creativecommons.org/licenses/by-nc-nd/4.0

Figure 5. Developing the beating cardiac structure and endothelial network in extended-cultured gastruloids

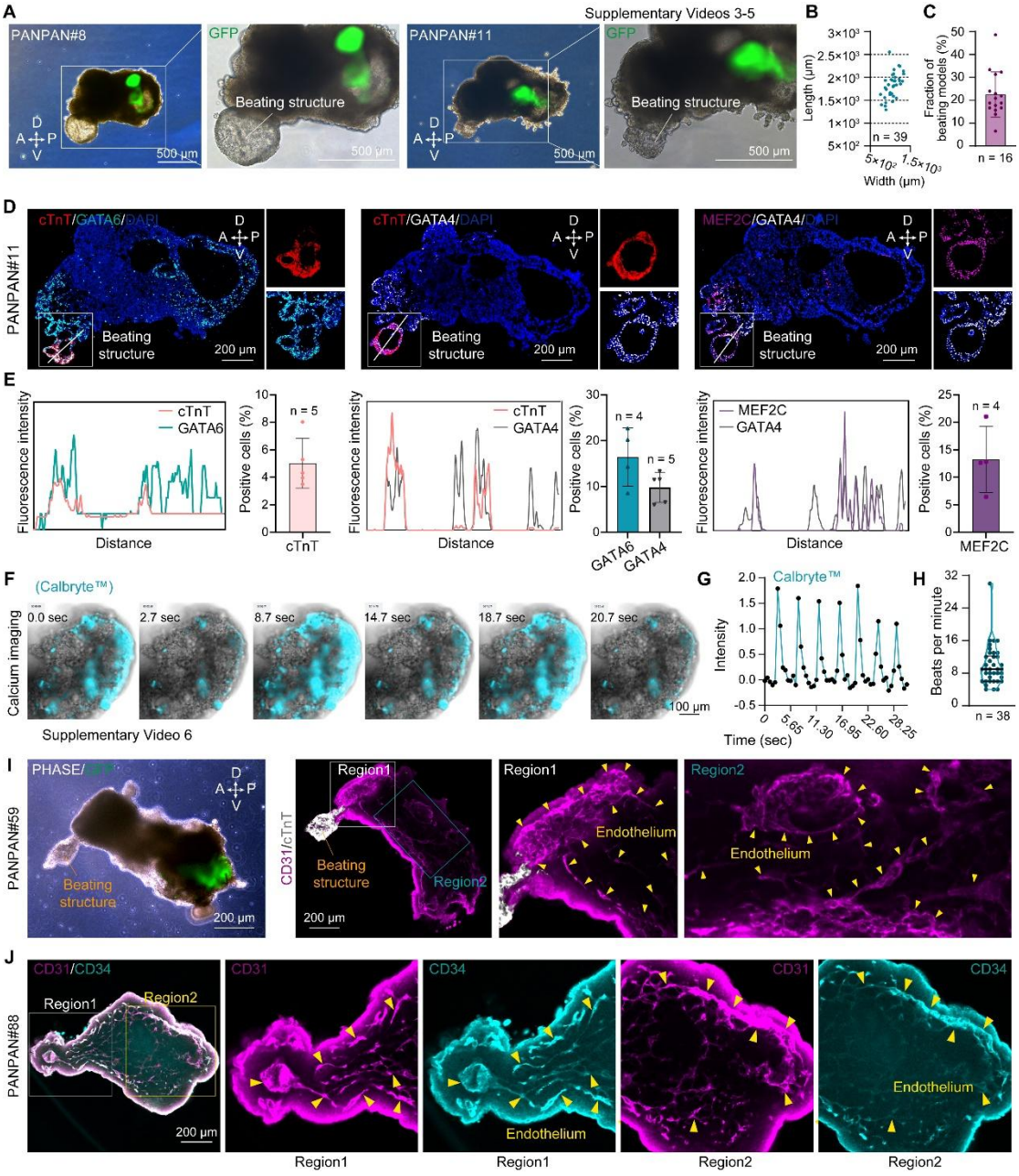

(A) Representative merged fluorescence and bright field images of gastruloids with a beating structure. The beating gastruloid is labeled “PANPAN.”
(B) Length and width measurements of PANPANs.
(C) Percentage of beating gastruloids across multiple independent experiments.
(D) IF images showing expression of cardiac markers cTnT, GATA4, GATA6, and MEF2C.
(E) Line scans showing the fluorescence intensities of these markers along the white arrow line in the merged panel from (D). The bar graph showing the positive rates of the indicated markers.
(F) Calcium imaging of a beating domain using a Calbryte™ dye.
(G) Intensity profile of Calbryte™ fluorescence showing rhythmic calcium

Langtaosha (LTS) Preprint doi: https://doi.org/10.65215/LTSpreprints.2026.08.25.000317. This version posted August 26, 2026. The copyright holder for this preprint (which was not certified by peer review) is the author/funder. Creative Commons license: CC Attribution-NonCommercial-NoDerivatives 4.0 https://creativecommons.org/licenses/by-nc-nd/4.0

oscillations within beating domains.
(H) Beats per minute measurement of PANPANs.
(I) IF images showing expression of cardiac marker cTnT and endothelial marker CD31. Yellow triangles indicate CD31-positive endothelial networks.
(J) IF images showing expression of endothelia markers CD31 and CD34. Yellow triangles indicate CD31/CD34 double-positive endothelial networks.

Langtaosha (LTS) Preprint doi: https://doi.org/10.65215/LTSpreprints.2026.08.25.000317. This version posted August 26, 2026. The copyright holder for this preprint (which was not certified by peer review) is the author/funder. Creative Commons license: CC Attribution-NonCommercial-NoDerivatives 4.0 https://creativecommons.org/licenses/by-nc-nd/4.0

716 # STAR METHODS

717 ## KEY RESOURCES TABLE

REAGENT or RESOURCE	Source	Identifier
Antibodies		
Goat anti-GSC	R&D Systems	Cat#AF4086; RRID:AB_2114650
Rabbit anti-NOGGIN	Abcam	Cat#ab16054; RRID:AB_470248
Rabbit anti-FOXA2	Cell Signaling Technology	Cat# 8186S; RRID:AB_10891055
Rat anti-SOX2	Thermo Fisher Scientific	Cat#14-9811-82; RRID:AB_11219471
Mouse anti-OCT4	Cell Signaling Technology	Cat#75463S; RRID:AB_2799870
Rabbit anti-NANOG	Cell Signaling Technology	Cat#4903S; RRID:AB_10559205
Rabbit anti-HOXB9	Cell Signaling Technology	Cat#27967S
Rabbit anti-CDX2	Abcam	Cat#AB76541; RRID:AB_1523334
Goat anti-TBXT	R&D Systems	Cat#AF2085; RRID:AB_2200235
Rabbit anti-MIXL1	Proteintech	Cat#22772-1-AP; RRID:AB_2879164
Rabbit anti-EOMES	Abcam	Cat#ab23345; RRID:AB_778267
Rabbit anti-E-CAD	Cell Signaling Technology	Cat#3195S; RRID:AB_2291471
Mouse anti-N-CAD	Cell Signaling Technology	Cat#14215S; RRID:AB_2798427
Goat anti-TBX6	R&D Systems	Cat#AF4744; RRID:AB_2200834
Rabbit anti-LHX1	Abcam	Cat#ab229474;

Langtaosha (LTS) Preprint doi: https://doi.org/10.65215/LTSpreprints.2026.08.25.000317. This version posted August 26, 2026. The copyright holder for this preprint (which was not certified by peer review) is the author/funder. Creative Commons license: CC Attribution-NonCommercial-NoDerivatives 4.0 https://creativecommons.org/licenses/by-nc-nd/4.0

		RRID:AB_2924798
Goat anti-HAND1	R&D Systems	Cat#AF3168; RRID:AB_2115853
Rabbit anti-HAND2	Novus Biologicals	Cat#NBP2-58062; RRID:AB_3343042
Rabbit anti-FOXF1	Abcam	Cat#ab168383; RRID:AB_3676395
Rabbit anti-LUM	Abcam	Cat#ab168348; RRID:AB_2920864
Rabbit anti-ANXA1	R&D Systems	Cat# AB214486; RRID:AB_2890907
Rat anti-POSTN	R&D Systems	Cat#MAB3548; RRID:AB_2252599
Mouse anti-SOX17	BD Biosciences	Cat#561590; RRID:AB_10717127
Goat anti-SOX17	R&D Systems	Cat#AF1924; RRID:AB_355060
Rabbit anti-GATA6	Abcam	Cat#ab175927
anti-GATA4	Santa Cruz Biotechnology	Cat# sc-25310, RRID:AB_627667
Goat anti-LHX5	R&D Systems	Cat#AF6290; RRID:AB_10973257
Rabbit anti-PAX6	Abcam	Cat#ab195045; RRID:AB_2750924
Goat anti-SOX3	R&D Systems	Cat#AF2569; RRID:AB_2239933
Rabbit anti-FOXG1	Cell Signaling Technology	Cat# 29642T
Rabbit anti-OTX2	Proteintech	Cat#13497-1-AP; RRID:AB_2157176
Goat anti-OTX2	R&D Systems	Cat#AF1979; RRID:AB_2157172
Goat anti-SOX1	R&D Systems	Cat#AF3369; RRID:AB_2239879
Rabbit anti-SIX3	Cell Signaling	Cat#62173T

Langtaosha (LTS) Preprint doi: https://doi.org/10.65215/LTSpreprints.2026.08.25.000317. This version posted August 26, 2026. The copyright holder for this preprint (which was not certified by peer review) is the author/funder. Creative Commons license: CC Attribution-NonCommercial-NoDerivatives 4.0 https://creativecommons.org/licenses/by-nc-nd/4.0

	Technology	
Goat anti-SOX10	R&D Systems	Cat#AF2864; RRID:AB_442208
Rabbit anti-SOX9	Abcam	Cat#ab185966; RRID:AB_2728660
Mouse anti-cTnT	Thermo Fisher Scientific	Cat#MA5-12960; RRID:AB_11000742
Rabbit anti-cTnT	Abcam	Cat#ab209813; RRID:AB_2938619
Rabbit anti-MEF2C	Cell Signaling Technology	Cat#5030S; RRID:AB_10548759
Rabbit anti-PECAM1 (CD31)	Proteintech	Cat# 11265-1-AP; RRID:AB_2299349
Mouse anti-CD34	Thermo Fisher Scientific	Cat#MA1-10202; RRID:AB_11156010
Goat anti-SHH	R&D Systems	Cat#AF464; RRID:AB_355373
Donkey anti-Goat IgG (H+L) Alexa Fluor™ Plus 647	Thermo Fisher Scientific	Cat#A32849; RRID:AB_2762840
Donkey anti-Goat IgG (H+L) Alexa Fluor™ Plus 555	Thermo Fisher Scientific	Cat#A32816; RRID:AB_2762839
Donkey anti-Rabbit IgG (H+L) Alexa Fluor™ Plus 647	Thermo Fisher Scientific	Cat#A32795; RRID:AB_2762835
Donkey anti-Rabbit IgG (H+L) Alexa Fluor™ Plus 555	Thermo Fisher Scientific	Cat#A32794; RRID:AB_2762834
Donkey anti-Rabbit IgG (H+L) Alexa Fluor™ Plus 488	Thermo Fisher Scientific	Cat#A32790; RRID:AB_2762833
Donkey anti-Mouse IgG (H+L) Alexa	Thermo Fisher Scientific	Cat#A32787; RRID:AB_2762830

Langtaosha (LTS) Preprint doi: https://doi.org/10.65215/LTSpreprints.2026.08.25.000317. This version posted August 26, 2026. The copyright holder for this preprint (which was not certified by peer review) is the author/funder. Creative Commons license: CC Attribution-NonCommercial-NoDerivatives 4.0 https://creativecommons.org/licenses/by-nc-nd/4.0

Fluor™ Plus 647		
Donkey anti-Mouse IgG (H+L) Alexa Fluor™ Plus 555	Thermo Fisher Scientific	Cat#A32773; RRID:AB_2762848
Donkey anti-Mouse IgG (H+L) Alexa Fluor™ Plus 488	Thermo Fisher Scientific	Cat#A32766; RRID:AB_2762823
Donkey anti-Mouse IgG (H+L) Alexa Fluor™ Plus 405	Thermo Fisher Scientific	Cat#A48257; RRID:AB_2884884
Donkey anti-Rat IgG (H+L) Alexa Fluor™ Plus 555	Thermo Fisher Scientific	Cat#A48270; RRID:AB_2896336
Donkey anti-Rat IgG (H+L) Alexa Fluor™ Plus 405	Thermo Fisher Scientific	Cat#A48268; RRID:AB_2890549
Chemicals, peptides, and recombinant proteins		
mTeSR Plus	STEMCELL Technologies	Cat#100-0276
DMEM/F12	Gibco	Cat#C11330500BT
MEM NEAA	Gibco	Cat#11140050
Matrigel	Corning	Cat#354234
TrypLE Express	Gibco	Cat#12604021
ReLeSR™	STEMCELL Technologies	Cat#100-0484
N-2	Gibco	Cat#17502048
B-27	Gibco	Cat#17504044

Langtaosha (LTS) Preprint doi: https://doi.org/10.65215/LTSpreprints.2026.08.25.000317. This version posted August 26, 2026. The copyright holder for this preprint (which was not certified by peer review) is the author/funder. Creative Commons license: CC Attribution-NonCommercial-NoDerivatives 4.0 https://creativecommons.org/licenses/by-nc-nd/4.0

Y27632	TargetMol	Cat#T1725
CHIR99021	TargetMol	Cat#T2310
Activin A	Novoprotein	Cat#C687
anti-adhesion solution	STEMCELL Technologies	Cat#07010
Tissue-clearing reagent CUBIC-L	Tokyo Chemical Industry	Cat#T3740
Tissue-clearing reagent CUBIC-R	Tokyo Chemical Industry	Cat#T3741
RNAzol® RT	MOLECULAR RESEARCH CENTER, INC.	Cat#RN190
All-in-one 1st Strand cDNA Synthesis SuperMix	Novoprotein	Cat#E047
2x Taq Pro Universal SYBR qPCR Master Mix	Vazyme	Cat#Q712
BD Rhapsody™ Cartridge Reagent Kit	BD Biosciences	Cat#633731
BD Rhapsody™ Cartridge Kit	BD Biosciences	Cat#633733
BD Rhapsody™ cDNA Kit	BD Biosciences	Cat#633773
BD Human Single-Cell Multiplexing Kit	BD Biosciences	Cat#633781
BD Rhapsody™ WTA Amplification Kit	BD Biosciences	Cat#633801
Phalloidin Labeling	Thermo Fisher	Cat#A34055

Langtaosha (LTS) Preprint doi: https://doi.org/10.65215/LTSpreprints.2026.08.25.000317. This version posted August 26, 2026. The copyright holder for this preprint (which was not certified by peer review) is the author/funder. Creative Commons license: CC Attribution-NonCommercial-NoDerivatives 4.0 https://creativecommons.org/licenses/by-nc-nd/4.0

Probes	Scientific	
NucSpot® Live Cell Nuclear Stains	Biotium	Cat#40082-T
Calbryte™ 520	AAT Bioquest	Cat#20650
Deposited Data		
scRNA-seq	This study	
scRNA-seq of CS7 human embryo	Tyser et al.[44]	E-MTAB-9388
scRNA-seq of CS8 human embryo	Xiao et al.[45]	HRA005567
scRNA-seq of CS10 human embryo	Zeng et al.[47]	GSE155121
scRNA-seq of CS12 human embryo	Xu et al.[46]	GSE157329
scRNA-seq of gastrulating monkey embryo	Zhai et al.[62]	GSE193007
scRNA-seq of gastrulating mouse embryo	Pijuan-Sala et al.[73]	E-MTAB-6967
scRNA-seq of the peri-gastruloid	Liu et al.[18]	
scRNA-seq of synthetic embryos model (SEM)	Oldak et al.[15]	GSE193007
Experimental models: cell lines		
H1 hESC (WA01)	WiCell	RRID: CVCL_9771
H9 hESC (WA09)	WiCell	RRID: CVCL_9773
RUES2-GLR	The Rockefeller University (RUES)	RUESe002-A-6
GFP-H1 hESC	This study	GFP
Oligonucleotides		
Primers, See Table S1	Sangon Biotech	
Software and		

Langtaosha (LTS) Preprint doi: https://doi.org/10.65215/LTSpreprints.2026.08.25.000317. This version posted August 26, 2026. The copyright holder for this preprint (which was not certified by peer review) is the author/funder. Creative Commons license: CC Attribution-NonCommercial-NoDerivatives 4.0 https://creativecommons.org/licenses/by-nc-nd/4.0

algorithms		
FastQC (v0.11.9)	N/A	https://www.bioinformatics.babraham.ac.uk/projects/fastqc
MultiQC (v1.13)	Ewels et al.[115]	https://multiqc.info
STAR (v2.7.9a)	Dobin et al.[116]	https://github.com/alexdobin/STAR
BD Rhapsody (v2.0b1)	N/A	https://www.bdbiosciences.com
R (v4.2.1)	N/A	https://www.R-project.org
Python (v3.8)	N/A	https://www.python.org
Seurat (v4.3.0)	Stuart et al.[117]	https://satijalab.org/seurat
Harmony (v0.1.1)	Korsunsky et al.[118]	https://portals.broadinstitute.org/harmony
SCP (v 0.5.4)	N/A	https://github.com/zhanghao-njmu/SCP
ggplot2 (v3.4.2)	N/A	https://github.com/tidyverse/ggplot2
ComplexHeatmap (v 2.14.0)	Gu et al.[119]	https://jokergoo.github.io/ComplexHeatmap-reference/book/
Other		
AggreWell™400 24-well plate	STEMCELL Technologies	Cat#34415
Ultra-Low Cluster,96 Well	Costar	Cat#7007

EXPERIMENTAL MODEL AND SUBJECT DETAILS

Ethics statement

This research was approved by the Ethics Committee of Zhongshan School of Medicine at Sun Yat-sen University and the Ethics Committee of the Seventh Affiliated Hospital of Sun Yat-sen University. All procedures involving human pluripotent stem cells and human embryo models were conducted in accordance with applicable institutional policies, national regulations, and the 2025 Guidelines for Stem Cell Research and Clinical Translation issued by the International Society for Stem Cell Research (ISSCR). Human pluripotent stem cells used in this study were obtained ethically and in compliance with the relevant regulations and guidelines established by Sun Yat-sen University, the Ministry of Science and Technology, and the Ministry of Health of the People's Republic of China. The embryo models generated in this study were intentionally incomplete, lacking key extraembryonic lineages, including trophoblast and hypoblast populations, and therefore do not have the potential

Langtaosha (LTS) Preprint doi: https://doi.org/10.65215/LTSpreprints.2026.08.25.000317. This version posted August 26, 2026. The copyright holder for this preprint (which was not certified by peer review) is the author/funder. Creative Commons license: CC Attribution-NonCommercial-NoDerivatives 4.0 https://creativecommons.org/licenses/by-nc-nd/4.0

to support complete human development. *Xenopus* embryo usage was minimized throughout the study, and no *Xenopus*–human chimeric embryos were allowed to develop beyond the approved experimental stages.

Stem cell culture

Human pluripotent stem cell (hPSC) lines (H1, H9, and RUES2-GLR[48]) were cultured on feeder-free Matrigel (Corning)-coated culture plates, with daily mTeSR Plus medium (STEMCELL Technologies) changes. During cell passaging, the cells were dissociated using ReLeSR™ (STEMCELL Technologies) for 2-5 minutes at room temperature. Following the removal of reagent, cells were resuspended in fresh mTeSR Plus medium and gently pipetted to dissociate residual aggregates. A 10–20% fraction of dissociated cells was routinely passaged to new Matrigel-coated plates and cultured at 37°C in a humidified 5% CO_2 incubator. Mycoplasma contamination was routinely monitored by PCR.

METHOD DETAILS

Generation of signaling center from human pluripotent stem cells

hPSCs were dissociated into single cells using TrypLE and subsequently transferred into AggreWell 400 plates (24-well format; STEMCELL Technologies). Before cell seeding, each well was coated with 500 μL of anti-adhesion solution (STEMCELL Technologies), and the plate was centrifuged at 1300 g for 7 min to ensure even coating of the well bottom and remove air bubbles. The anti-adhesion solution was left on the AggreWell at room temperature for 15 min. Concurrently, hPSC clones were washed twice with PBS to eliminate floating dead cells. In a 6-well plate, 500 μL of TrypLE was added to each well, covering the bottom, and incubated for 2-3 min to dissociate clones into single cells. Gentle tapping of the 6-well plate was performed to enhance dissociation, followed by transferring the single-cell suspension to a 15 mL centrifuge tube. Next, 10 times the volume of PBS was added to the tube, and the mixture was centrifuged at 300 g for 4 min. After discarding the supernatant, the single cells were resuspended in signaling activation medium (DMEM/F12 basal medium (Gibco) containing 0.5% N2 (Gibco), 1% B27 (Gibco), 1% nonessential amino acids (NEAA; Gibco), 3 μM CHIR (TargetMol) and 100 ng/mL Activin A (Novoprotein). In parallel, cells were cultured in medium containing either 3 μM CHIR alone, 100 ng/mL Activin A alone, or 50 ng/mL BMP4 (Novoprotein) alone. All conditions were supplemented with 10

Langtaosha (LTS) Preprint doi: https://doi.org/10.65215/LTSpreprints.2026.08.25.000317. This version posted August 26, 2026. The copyright holder for this preprint (which was not certified by peer review) is the author/funder. Creative Commons license: CC Attribution-NonCommercial-NoDerivatives 4.0 https://creativecommons.org/licenses/by-nc-nd/4.0

μM Y27632 (TargetMol). The anti-adhesion solution on the AggreWell was removed, and the plate was washed twice with signaling activation medium. The single-cell suspension was seeded into the pre-treated AggreWell at a density of 30,000 cells per well and supplemented with 2 mL of signaling activation medium containing 10 μM Y27632. The AggreWell plate was centrifuged at 100 g for 3 min to facilitate aggregation of approximately 25 cells per microwell at the well bottom. Subsequently, this AggreWell plate was cultured at 37°C in a humidified 5% CO_2 incubator. During daily medium changes, 1 mL of old medium was aspirated, and 1 mL of fresh signaling activation medium was slowly added along the well walls. The signaling center spheres used for *Xenopus* embryo transplantation and constructing the human gastruloid in this experiment were obtained from cells induced for 48 hours.

Self-organization of hPSC into 3D epiblast-like aggregates

hPSCs were dissociated into single cells using TrypLE and then suspended in N2B27 medium (consisting of DMEM/F12 basal medium with 0.5% N2 supplement, 1% B27 supplement, and 1% NEAA) along with 10 μM Y27632. The single cells were seeded into a 96-well clear round bottom ultra-low attachment microplate (Corning) at about 200-300 cells per well, and N2B27 medium with 10 μM Y27632 was added to each well, reaching a final volume of 100 μL. The plate was then centrifuged at 100 g for 3 min to promote aggregation of the cells at the well bottom. Subsequently, the 96-well plate was cultured in a humidified incubators at 37°C with 5% CO_2 and 5% O_2. The epiblast-like aggregates were obtained within 24 hours.

Generation of gastruloid

Upon harvesting, the signaling center spheres from the AggreWell were aspirated and transferred to 15 mL centrifuge tubes. The tubes were then centrifuged at 40 g for 30 s, and the supernatant was discarded. Immediately, 5 mL of N2B27 medium was added to each centrifuge tube, and another centrifugation at 40 g for 30 s was performed. The supernatant was then discarded, and this washing step was repeated 3 times to ensure removal of dead cells and the induction medium. Next, the signaling center spheres were resuspended in 3 mL of N2B27 medium and transferred to a 6-well plate. Using a micropipette under visual inspection, one signaling center sphere was gently aspirated and transferred to each well containing an epiblast-like aggregate in a 96-well plate. After transferring the signaling center spheres to all the wells, 100 μL of N2B27 medium was added to each well. The plate was then

Langtaosha (LTS) Preprint doi: https://doi.org/10.65215/LTSpreprints.2026.08.25.000317. This version posted August 26, 2026. The copyright holder for this preprint (which was not certified by peer review) is the author/funder. Creative Commons license: CC Attribution-NonCommercial-NoDerivatives 4.0 https://creativecommons.org/licenses/by-nc-nd/4.0

centrifuged at 100 g for 3 minutes, facilitating the settling of both the signaling center sphere and epiblast-like aggregate at the bottom and promoting their attachment. The 96-well plate was placed inside a humidified incubator at 37°C with 5% CO_2 and 5% O_2. Every other day, a medium change was performed by aspirating 100 µL of the old medium from each well and subsequently adding 100 µL of fresh N2B27 medium.

Immunofluorescence staining and imaging

The gastruloids at different developmental stages were collected from the 96-well plates into 15 mL centrifuge tubes. After washing twice with PBS, they were fixed with 4% paraformaldehyde (PFA) at 4°C overnight.

To perform cryosectioning, the fixed samples were washed 3 times with PBS at room temperature, embedded in OCT compound (Sakura), and frozen at -80°C. Cryosections were made at a thickness of 15 µm, and the resulting tissue section was placed on adhesion microscope slides (Citotest). Sample slides were then stored at -80°C. Before conducting the staining procedures, antigen retrieval was performed by heating slides at 95°C for 10 min in EDTA Antigen Retrieval Solution (pH 8.0) (Sangon Biotech).

To perform tissue clearing, the fixed samples were washed 3 times with PBS and soaked in CUBIC-L (Tokyo Chemical Industry), a delipidation and decoloring reagent. The samples were placed on a rotator at 37°C for 3-7 days, with daily replacement of fresh CUBIC-L. Before proceeding with immunofluorescence staining, the delipidated samples were washed three times with PBS.

For immunofluorescence staining, all samples (sections or cleared gastruloids) were blocked with PBST-BSA (PBS + 0.1% Triton X-100, containing 5% bovine serum albumin (BSA)) at room temperature for 1-2 hours. The primary antibody was diluted in PBST-BSA and incubated with the samples overnight at 4°C. Following incubation, the samples were washed five times with PBS to remove the primary antibody. Subsequently, the samples were incubated at room temperature with the secondary antibody and DAPI (Roche), both diluted in PBST-BSA for 1 hour. After washing the samples five times with PBS, they were imaged by microscopy.

Imaging was performed on Zeiss Inverted LSM 780/880 laser scanning confocal microscopes, or a Dragonfly CR-DFLY-202 2540 upright confocal microscope, or Lightsheet microscope (Bruker Trulive3D Imager), or an inverted microscope Leica DMi8. The Z-stack images acquired using the confocal scanning or Lightsheet microscopes were then processed and

Langtaosha (LTS) Preprint doi: https://doi.org/10.65215/LTSpreprints.2026.08.25.000317. This version posted August 26, 2026. The copyright holder for this preprint (which was not certified by peer review) is the author/funder. Creative Commons license: CC Attribution-NonCommercial-NoDerivatives 4.0 https://creativecommons.org/licenses/by-nc-nd/4.0

integrated using Imaris (v9.8.2) to achieve the 3D reconstruction of the gastruloid structures.

Generation of human-*Xenopus* chimeric embryos.

For microinjection, the untreated and CHIR/Activin A instructed GFP-hPSCs were dissociated into single cells by TrypLE, centrifuged at 300 g for 4 minutes. After supernatant removal, the cell pellet was resuspended in N2B27 medium and adjusted to a final concentration of 5×10^7 cells/mL. The cell suspensions were loaded into a prepared injection needle (WPI, 1B100F-4) by microloader (Eppendorf, 5242956003). Approximately 30-40 nL of cell suspensions or PBS were microinjected into the ventral side of stage 9 *Xenopus* embryos. After injection, embryos were allowed to develop for about 20 h at a constant temperature of 23°C. The embryo morphology and fluorescence expression were analyzed using a stereomicroscope (Leica M205FA). Subsequently, all the embryos were fixed by 4% PFA and subjected to hematoxylin-eosin (HE) staining or optical clearing, followed by fluorescence imaging for visualization of the ectopic axis formation.

Calcium imaging

Calcium transients were recorded in PANPANs (gastruloids developing a beating structure) that exhibited spontaneous contractility. Samples were incubated with 1 mM Calbryte™ 590 AM (AAT Bioquest, #20700) in Dulbecco's phosphate buffered saline (DPBS, Thermo Fisher Scientific) for 30 min at 37°C, followed by two washes with pre-warmed DMEM/F-12 basal medium (Corning). Stained PANPANs were transferred to a 6-well cell culture plate (NEST) and imaged on a Nikon Ti2-E microscope. Fluorescence intensity was quantified using NIS-Elements AR software (version6.02.02).

Live imaging

Live imaging was performed using NucSpot® Live 650 nuclear dye (Biotium, 40082). Day 1 gastruloids in 96-well plates were incubated with 1x NucSpot® Live 650 (Biotium, 40082) in fresh N2B27 medium for 30 min at 37°C under 5% CO2. Confocal imaging was conducted on Olympus SpinSR10 spinning disk confocal microscope, using 488nm and 640nm excitation. Images were acquired every 10 min, with cell viability maintained via a stage top incubator (Tokai Hit).

Langtaosha (LTS) Preprint doi: https://doi.org/10.65215/LTSpreprints.2026.08.25.000317. This version posted August 26, 2026. The copyright holder for this preprint (which was not certified by peer review) is the author/funder. Creative Commons license: CC Attribution-NonCommercial-NoDerivatives 4.0 https://creativecommons.org/licenses/by-nc-nd/4.0

RNA extraction and RT-PCR analysis

Total RNA was extracted using RNAzol (Molecular Research Center, Inc.) following the manufacturer's protocol, and then reverse transcribed into cDNA using an All-in-one 1st Strand cDNA Synthesis SuperMix kit (Novoprotein). For qRT-PCR, a 2x Taq Pro Universal SYBR qPCR Master Mix (Vazyme) was utilized on a LightCycler 480 Detection System (Roche). The thermocycling conditions comprised 40 cycles of denaturation at 95°C for 10 s, annealing at 60°C for 10 s, and extension at 72°C for 10 s. The primers are listed in supplementary table S1. *GAPDH* was used as an internal control, and gene expression levels were calculated relative to *GAPDH* or using the $2^{-\Delta\Delta CT}$ method.

Construction of the Single-cell library

Gastruloids were dissociated into single cells by treating with 1× TrypLE for 15-30 min at 37°C. PBS was added to terminate the enzymatic reaction and the cells were centrifuged at 300 g for 5 min at 4°C, followed by the resuspension with 1 mL pre-cold 0.1% BSA-PBS.

For multiplexing, samples were labeled using the BD Human Single-Cell Multiplexing Kit (BD Biosciences) on ice for 30 minutes. After labeling, the samples were pooled and washed twice with 0.1% BSA-PBS for library preparation. The single cell libraries were generated using the BD Rhapsody system with the BD Rhapsody™ cDNA Kit (BD Biosciences) and BD Rhapsody™ WTA Amplification Kit (BD Biosciences), following the manufacturer's protocol. Subsequently, the libraries were pooled and then delivered to the medical inspection laboratories (Annoroad Gene Technology) for sequence by Novaseq.

BD scRNA-seq data processing

Raw FASTQ files generated from the BD single-cell RNA-seq platform were first checked by FastQC (release 0.11.9), and its results were then parsed by MultiQC (release 1.13)[115]. Next, FASTQ files were processed using the BD Rhapsody pipeline (version 2.0b1) wrapped in a Docker container (bdgenomics/rhapsody) and executed via cwlref-runner (version 1.0). To enable accurate quantification of an exogenous GFP transcript expressed in the cells, the GFP sequence was manually appended to the GRCh38 reference genome, and the corresponding annotation was added to the GTF file. A customized genome index was then built using STAR. During analysis, the pipeline performed adapter trimming, quality filtering, and extraction of cell barcodes and unique molecular identifiers (UMIs). Filtered reads were aligned to the

Langtaosha (LTS) Preprint doi: https://doi.org/10.65215/LTSpreprints.2026.08.25.000317. This version posted August 26, 2026. The copyright holder for this preprint (which was not certified by peer review) is the author/funder. Creative Commons license: CC Attribution-NonCommercial-NoDerivatives 4.0 https://creativecommons.org/licenses/by-nc-nd/4.0

customized reference genome, and gene-level quantification was conducted by collapsing UMIs to remove PCR duplicates and counting reads uniquely mapped to annotated gene loci, resulting in a gene-by-cell count matrix.

Downstream analysis of scRNA-seq data

The Seurat toolkit (release 4.3.0)[117] was used to perform downstream analysis. First, high-quality single-cell transcriptomes were retained via stringent quality control thresholds (500 < nFeature_RNA < 7000, 1000 < nCount_RNA < 40000, percent.mt < 25%). The upper limit of nFeature_RNA and nCount_RNA was specifically set to remove putative doublets. Then, the raw count data were normalized and scaled using “NormalizeData” and “ScaleData” sub-functions. We performed principal component analysis (PCA) on the top 2000 highly variable genes (HVGs) with ‘‘RunPCA’. The significant principal components were selected according to the p-values and standard deviation dynamics. Cells were then clustered utilizing the ‘‘FindClusters’’. The clustered cells were then projected onto a two-dimensional space using “RunUMAP”. To annotate cells, we first identified the specifically expressed genes on each cluster. The cells were then manually annotated by curated known cell markers. Integrating single-cell data across experiments, including data generated in this study and accessed from public dataset, was performed by R package Harmony (release 0.1.1)[118].

Identification of cluster-specific marker genes

To identify marker genes specific to each cell type, we employed the “cosg” function implemented in the COSG R package (version 0.9.0)[120]. To evaluate the similarity between marker gene sets across different clusters, we computed pairwise Jaccard indices, defined as the size of the intersection divided by the size of the union of marker gene sets between any two cell types. A Jaccard similarity matrix was constructed and visualized using the R package ComplexHeatmap (version 2.14.0)[119], with hierarchical clustering applied to both rows and columns.

Cross-species and cross-model dataset integration and comparison

To enable integrative analysis across multiple species, single-cell RNA-seq datasets from human (CS7, CS8, and CS10), monkey (CS8), mouse (gastrulation stage), peri-gastruloid, and synthetic embryos model (SEM)[15,18,44,45,47,62,73], and our own dataset were integrated using the Seurat v4

Langtaosha (LTS) Preprint doi: https://doi.org/10.65215/LTSpreprints.2026.08.25.000317. This version posted August 26, 2026. The copyright holder for this preprint (which was not certified by peer review) is the author/funder. Creative Commons license: CC Attribution-NonCommercial-NoDerivatives 4.0 https://creativecommons.org/licenses/by-nc-nd/4.0

framework. For each dataset, raw counts were normalized and 2,000 highly variable genes were identified using the variance stabilizing transformation (VST) method. Integration anchors were computed using the FindIntegrationAnchors function in Seurat package with the top 20 principal components, followed by data integration using IntegrateData. The integrated object was scaled, and dimensionality reduction was performed using PCA (30 components) and UMAP (based on the first 20 PCs). Integrated datasets were visualized by UMAP, and cells were colored by annotated cell types and split by dataset for comparative interpretation. To quantify the similarity of cell type compositions across datasets, we applied the SCP package (version 0.5.4) to compute cell-type correlation heatmaps. Specifically, the CellCorHeatmap function was used to calculate correlations between cell types in our dataset and the public datasets, based on average gene expression.

Langtaosha (LTS) Preprint doi: https://doi.org/10.65215/LTSpreprints.2026.08.25.000317. This version posted August 26, 2026. The copyright holder for this preprint (which was not certified by peer review) is the author/funder. Creative Commons license: CC Attribution-NonCommercial-NoDerivatives 4.0 https://creativecommons.org/licenses/by-nc-nd/4.0

PEFERENCES

1. Schoenwolf, G.C., Bleyl, S.B., Brauer, P.R., and Francis-West, P.H. (2014). Larsen's human embryology (Elsevier Health Sciences).
2. Wolpert, L., Tickle, C., and Arias, A.M. (2015). Principles of development (Oxford University Press, USA).
3. Hyun, I., Wilkerson, A., and Johnston, J. (2016). Embryology policy: Revisit the 14-day rule. Nature *533*, 169-171.
4. Nájera, G.S., and Weijer, C.J. (2023). The evolution of gastrulation morphologies. Development *150*.
5. Lee, K.Y., and DeMayo, F.J. (2004). Animal models of implantation. Reproduction *128*, 679-695.
6. Liu, L., and Wu, J. (2025). Stem cell-based models of early human development. Development *152*, dev204543.
7. Shahbazi, M.N., and Pasque, V. (2024). Early human development and stem cell-based human embryo models. Cell Stem Cell *31*, 1398-1418.
8. Yu, L., Wei, Y., Duan, J., Schmitz, D.A., Sakurai, M., Wang, L., Wang, K., Zhao, S., Hon, G.C., and Wu, J. (2021). Blastocyst-like structures generated from human pluripotent stem cells. Nature *591*, 620-626.
9. Kagawa, H., Javali, A., Khoei, H.H., Sommer, T.M., Sestini, G., Novatchkova, M., Scholte op Reimer, Y., Castel, G., Bruneau, A., and Maenhoudt, N. (2022). Human blastoids model blastocyst development and implantation. Nature *601*, 600-605.
10. Liu, X., Tan, J.P., Schröder, J., Aberkane, A., Ouyang, J.F., Mohenska, M., Lim, S.M., Sun, Y.B., Chen, J., and Sun, G. (2021). Modelling human blastocysts by reprogramming fibroblasts into iBlastoids. Nature *591*, 627-632.
11. Yanagida, A., Spindlow, D., Nichols, J., Dattani, A., Smith, A., and Guo, G. (2021). Naive stem cell blastocyst model captures human embryo lineage segregation. Cell Stem Cell *28*, 1016-1022 e1014.
12. Okubo, T., Rivron, N., Kabata, M., Masaki, H., Kishimoto, K., Semi, K., Nakajima-Koyama, M., Kunitomi, H., Kaswandy, B., and Sato, H. (2024). Hypoblast from human pluripotent stem cells regulates epiblast development. Nature *626*, 357-366.
13. Pedroza, M., Gassaloglu, S.I., Dias, N., Zhong, L., Hou, T.J., Kretzmer, H., Smith, Z.D., and Sozen, B. (2023). Self-patterning of human stem cells into post-implantation lineages. Nature.
14. Weatherbee, B.A.T., Gantner, C.W., Iwamoto-Stohl, L.K., Daza, R.M., Hamazaki, N., Shendure, J., and Zernicka-Goetz, M. (2023). Pluripotent stem cell-derived model of the post-implantation human embryo. Nature.
15. Oldak, B., Wildschutz, E., Bondarenko, V., Comar, M.-Y., Zhao, C., Aguilera-Castrejon, A., Tarazi, S., Viukov, S., Pham, T.X.A., Ashouokhi, S.*, et al.* (2023). Complete human day 14 post-implantation embryo models from naive ES cells. Nature *622*, 562-573.
16. Hislop, J.J., Alavi, A., Song, Q., Schoenberger, R.L., Keshavarz, F.K., LeGraw, R., Velazquez, J.J., Mokhtari, T., Taheri, M.N., Rytel, M.*, et al.* (2023).

Langtaosha (LTS) Preprint doi: https://doi.org/10.65215/LTSpreprints.2026.08.25.000317. This version posted August 26, 2026. The copyright holder for this preprint (which was not certified by peer review) is the author/funder. Creative Commons license: CC Attribution-NonCommercial-NoDerivatives 4.0 https://creativecommons.org/licenses/by-nc-nd/4.0

Modelling Human Post-Implantation Development via Extra-Embryonic Niche Engineering. bioRxiv.

17. Ai, Z., Niu, B., Yin, Y., Xiang, L., Shi, G., Duan, K., Wang, S., Hu, Y., Zhang, C., and Zhang, C. (2023). Dissecting peri-implantation development using cultured human embryos and embryo-like assembloids. Cell Research *33*, 661-678.

18. Liu, L., Oura, S., Markham, Z., Hamilton, J.N., Skory, R.M., Li, L., Sakurai, M., Wang, L., Pinzon-Arteaga, C.A., Plachta, N.*, et al.* (2023). Modeling post-implantation stages of human development into early organogenesis with stem-cell-derived peri-gastruloids. Cell.

19. Shen, Q., Zhang, X., Chen, N., Yan, X., Ren, H., Sun, X., Xu, L., Zhao, J., Li, R., and Lin, S. (2026). Reconstituting human primitive streak formation through extra-embryonic cell coordination. Cell.

20. Moris, N., Anlas, K., van den Brink, S.C., Alemany, A., Schroder, J., Ghimire, S., Balayo, T., van Oudenaarden, A., and Martinez Arias, A. (2020). An in vitro model of early anteroposterior organization during human development. Nature *582*, 410-415.

21. Warmflash, A., Sorre, B., Etoc, F., Siggia, E.D., and Brivanlou, A.H. (2014). A method to recapitulate early embryonic spatial patterning in human embryonic stem cells. Nat Methods *11*, 847-854.

22. Wu, H., and Wang, H. (2026). Progress in stem cell-based embryo models and their applications in developmental biology and biomedicine. Nature Reviews Molecular Cell Biology, 1-16.

23. Abilez, O.J., Yang, H., Guan, Y., Shen, M., Yildirim, Z., Zhuge, Y., Venkateshappa, R., Zhao, S.R., Gomez, A.H., and El-Mokahal, M. (2025). Gastruloids enable modeling of the earliest stages of human cardiac and hepatic vascularization. Science *388*, eadu9375.

24. Yamanaka, Y., Hamidi, S., Yoshioka-Kobayashi, K., Munira, S., Sunadome, K., Zhang, Y., Kurokawa, Y., Ericsson, R., Mieda, A., Thompson, J.L.*, et al.* (2023). Reconstituting human somitogenesis in vitro. Nature *614*, 509-520.

25. Miao, Y., Djeffal, Y., De Simone, A., Zhu, K., Lee, J.G., Lu, Z., Silberfeld, A., Rao, J., Tarazona, O.A., Mongera, A.*, et al.* (2023). Reconstruction and deconstruction of human somitogenesis in vitro. Nature *614*, 500-508.

26. Hamazaki, N., Yang, W., Kubo, C.A., Qiu, C., Martin, B.K., Garge, R.K., Regalado, S.G., Nichols, E.K., Pendyala, S., Bradley, N.*, et al.* (2024). Retinoic acid induces human gastruloids with posterior embryo-like structures. Nat Cell Biol *26*, 1790-1803.

27. Rifes, P., Isaksson, M., Rathore, G.S., Aldrin-Kirk, P., Møller, O.K., Barzaghi, G., Lee, J., Egerod, K.L., Rausch, D.M., and Parmar, M. (2020). Modeling neural tube development by differentiation of human embryonic stem cells in a microfluidic WNT gradient. Nature biotechnology *38*, 1265-1273.

28. Karzbrun, E., Khankhel, A.H., Megale, H.C., Glasauer, S.M.K., Wyle, Y., Britton, G., Warmflash, A., Kosik, K.S., Siggia, E.D., Shraiman, B.I.*, et al.* (2021).

Langtaosha (LTS) Preprint doi: https://doi.org/10.65215/LTSpreprints.2026.08.25.000317. This version posted August 26, 2026. The copyright holder for this preprint (which was not certified by peer review) is the author/funder. Creative Commons license: CC Attribution-NonCommercial-NoDerivatives 4.0 https://creativecommons.org/licenses/by-nc-nd/4.0

Human neural tube morphogenesis in vitro by geometric constraints. Nature *599*, 268-272.

29. Hofbauer, P., Jahnel, S.M., Papai, N., Giesshammer, M., Deyett, A., Schmidt, C., Penc, M., Tavernini, K., Grdseloff, N., Meledeth, C.*, et al.* (2021). Cardioids reveal self-organizing principles of human cardiogenesis. Cell *184*, 3299-3317 e3222.

30. Schmidt, C., Deyett, A., Ilmer, T., Haendeler, S., Torres Caballero, A., Novatchkova, M., Netzer, M.A., Ceci Ginistrelli, L., Mancheno Juncosa, E., Bhattacharya, T.*, et al.* (2023). Multi-chamber cardioids unravel human heart development and cardiac defects. Cell *186*, 5587-5605 e5527.

31. Xue, X., Kim, Y.S., Ponce-Arias, A.-I., O'Laughlin, R., Yan, R.Z., Kobayashi, N., Tshuva, R.Y., Tsai, Y.-H., Sun, S., and Zheng, Y. (2024). A Patterned Human Neural Tube Model Using Microfluidic Gradients. Nature, 1-3.

32. Olmsted, Z.T., and Paluh, J.L. (2022). A combined human gastruloid model of cardiogenesis and neurogenesis. Iscience *25*.

33. Olmsted, Z.T., and Paluh, J.L. (2021). Co-development of central and peripheral neurons with trunk mesendoderm in human elongating multi-lineage organized gastruloids. Nature communications *12*, 3020.

34. Takebe, T., and Wells, J.M. (2019). Organoids by design. Science *364*, 956-959.

35. Wolpert, L. (1969). Positional information and the spatial pattern of cellular differentiation. J Theor Biol *25*, 1-47.

36. Spemann, H., and Mangold, H. (1924). über Induktion von Embryonalanlagen durch Implantation artfremder Organisatoren. Archiv für mikroskopische Anatomie und Entwicklungsmechanik *100*, 599-638.

37. De Robertis, E.M., Larrain, J., Oelgeschlager, M., and Wessely, O. (2000). The establishment of Spemann's organizer and patterning of the vertebrate embryo. Nat Rev Genet *1*, 171-181.

38. Capek, D., Smutny, M., Tichy, A.M., Morri, M., Janovjak, H., and Heisenberg, C.P. (2019). Light-activated Frizzled7 reveals a permissive role of non-canonical wnt signaling in mesendoderm cell migration. Elife *8*, e42093.

39. Manfrin, A., Tabata, Y., Paquet, E.R., Vuaridel, A.R., Rivest, F.R., Naef, F., and Lutolf, M.P. (2019). Engineered signaling centers for the spatially controlled patterning of human pluripotent stem cells. Nat Methods *16*, 640-648.

40. Sako, K., Pradhan, S.J., Barone, V., Ingles-Prieto, A., Muller, P., Ruprecht, V., Capek, D., Galande, S., Janovjak, H., and Heisenberg, C.P. (2016). Optogenetic Control of Nodal Signaling Reveals a Temporal Pattern of Nodal Signaling Regulating Cell Fate Specification during Gastrulation. Cell Rep *16*, 866-877.

41. Zheng, Y., Xue, X., Shao, Y., Wang, S., Esfahani, S.N., Li, Z., Muncie, J.M., Lakins, J.N., Weaver, V.M., Gumucio, D.L.*, et al.* (2019). Controlled modelling of human epiblast and amnion development using stem cells. Nature *573*, 421-425.

Langtaosha (LTS) Preprint doi: https://doi.org/10.65215/LTSpreprints.2026.08.25.000317. This version posted August 26, 2026. The copyright holder for this preprint (which was not certified by peer review) is the author/funder. Creative Commons license: CC Attribution-NonCommercial-NoDerivatives 4.0 https://creativecommons.org/licenses/by-nc-nd/4.0

42. Crease, D.J., Dyson, S., and Gurdon, J. (1998). Cooperation between the activin and Wnt pathways in the spatial control of organizer gene expression. Proceedings of the National Academy of Sciences *95*, 4398-4403.
43. Kremnyov, S., Lebedeva, T., Genikhovich, G., and Hejnol, A. (2026). A blastoporal organizer in a ctenophore. Nature *655*, 963-970.
44. Tyser, R.C.V., Mahammadov, E., Nakanoh, S., Vallier, L., Scialdone, A., and Srinivas, S. (2021). Single-cell transcriptomic characterization of a gastrulating human embryo. Nature *600*, 285-289.
45. Zhenyu, X., Lina, C., Yang, Y., Nannan, H., Xinwei, X., Sirui, L., Xiaolong, Y., Xin, Z., Peifu, S., Zhifeng, W.*, et al.* (2024). 3D reconstruction of a gastrulating human embryo. Cell.
46. Xu, Y., Zhang, T., Zhou, Q., Hu, M., Qi, Y., Xue, Y., Nie, Y., Wang, L., Bao, Z., and Shi, W. (2023). A single-cell transcriptome atlas profiles early organogenesis in human embryos. Nature cell biology *25*, 604-615.
47. Zeng, B., Liu, Z., Lu, Y., Zhong, S., Qin, S., Huang, L., Zeng, Y., Li, Z., Dong, H., Shi, Y.*, et al.* (2023). The single-cell and spatial transcriptional landscape of human gastrulation and early brain development. Cell Stem Cell *30*, 851-866 e857.
48. Martyn, I., Kanno, T.Y., Ruzo, A., Siggia, E.D., and Brivanlou, A.H. (2018). Self-organization of a human organizer by combined Wnt and Nodal signalling. Nature *558*, 132-135.
49. Naujok, O., Lentes, J., Diekmann, U., Davenport, C., and Lenzen, S. (2014). Cytotoxicity and activation of the Wnt/beta-catenin pathway in mouse embryonic stem cells treated with four GSK3 inhibitors. BMC Res Notes *7*, 273.
50. Bloise, E., Ciarmela, P., Dela Cruz, C., Luisi, S., Petraglia, F., and Reis, F.M. (2019). Activin A in Mammalian Physiology. Physiol Rev *99*, 739-780.
51. Sharon, N., Mor, I., Golan-lev, T., Fainsod, A., and Benvenisty, N. (2011). Molecular and functional characterizations of gastrula organizer cells derived from human embryonic stem cells. Stem Cells *29*, 600-608.
52. Cho, K.W., Blumberg, B., Steinbeisser, H., and De Robertis, E.M. (1991). Molecular nature of Spemann's organizer: the role of the Xenopus homeobox gene goosecoid. Cell *67*, 1111-1120.
53. Lemaire, P., and Kodjabachian, L. (1996). The vertebrate organizer: structure and molecules. Trends Genet *12*, 525-531.
54. Chawengsaksophak, K., de Graaff, W., Rossant, J., Deschamps, J., and Beck, F. (2004). Cdx2 is essential for axial elongation in mouse development. Proceedings of the National Academy of Sciences *101*, 7641-7645.
55. Favier, B., and Dolle, P. (1997). Developmental functions of mammalian Hox genes. Mol Hum Reprod *3*, 115-131.
56. Hobert, O., and Westphal, H. (2000). Functions of LIM-homeobox genes. Trends Genet *16*, 75-83.
57. Karvas, R.M., Zemke, J.E., Ali, S.S., Upton, E., Sane, E., Fischer, L.A., Dong, C., Park, K.M., Wang, F., Park, K.*, et al.* (2023). 3D-cultured blastoids model human embryogenesis from pre-implantation to early gastrulation stages.

Langtaosha (LTS) Preprint doi: https://doi.org/10.65215/LTSpreprints.2026.08.25.000317. This version posted August 26, 2026. The copyright holder for this preprint (which was not certified by peer review) is the author/funder. Creative Commons license: CC Attribution-NonCommercial-NoDerivatives 4.0 https://creativecommons.org/licenses/by-nc-nd/4.0

Cell Stem Cell *30*, 1148-1165 e1147.

58. Schüle, K.M., Weckerle, J., Probst, S., Wehmeyer, A.E., Zissel, L., Schröder, C.M., Tekman, M., Kim, G.-J., Schlägl, I.-M., and Arnold, S.J. (2023). Eomes restricts Brachyury functions at the onset of mouse gastrulation. Developmental Cell *58*, 1627-1642. e1627.

59. Sheng, G., Martinez Arias, A., and Sutherland, A. (2021). The primitive streak and cellular principles of building an amniote body through gastrulation. Science *374*, abg1727.

60. Keller, R. (2005). Cell migration during gastrulation. Curr Opin Cell Biol *17*, 533-541.

61. Chen, Q., Weng, K., Lin, M., Jiang, M., Fang, Y., Chung, S.S., Huang, X., Zhong, Q., Liu, Z., and Huang, Z. (2023). SOX9 modulates the transformation of gastric stem cells through biased symmetric cell division. Gastroenterology *164*, 1119-1136. e1112.

62. Zhai, J., Guo, J., Wan, H., Qi, L., Liu, L., Xiao, Z., Yan, L., Schmitz, D.A., Xu, Y., Yu, D.*, et al.* (2022). Primate gastrulation and early organogenesis at single-cell resolution. Nature *612*, 732-738.

63. Gong, Y., Bai, B., Sun, N., Ci, B., Shao, H., Zhang, T., Yao, H., Zhang, Y., Niu, Y., and Liu, L. (2023). Ex utero monkey embryogenesis from blastocyst to early organogenesis. Cell *186*, 2092-2110. e2023.

64. Zhai, J., Xu, Y., Wan, H., Yan, R., Guo, J., Skory, R., Yan, L., Wu, X., Sun, F., Chen, G.*, et al.* (2023). Neurulation of the cynomolgus monkey embryo achieved from 3D blastocyst culture. Cell *186*, 2078-2091 e2018.

65. Yuan, Y., Wang, X., Yan, X., He, N., Lu, X., Yang, J., Xie, X., Yuan, H., Chen, N., Liu, Y.*, et al.* (2025). 3D reconstruction of a human Carnegie stage 9 embryo provides a snapshot of early body plan formation. Cell Stem Cell.

66. Kumamoto, T., and Hanashima, C. (2017). Evolutionary conservation and conversion of Foxg1 function in brain development. Dev Growth Differ *59*, 258-269.

67. Peng, G., and Westerfield, M. (2006). Lhx5 promotes forebrain development and activates transcription of secreted Wnt antagonists. Development *133*, 3191-3200.

68. Simeone, A. (1998). Otx1 and Otx2 in the development and evolution of the mammalian brain. EMBO J *17*, 6790-6798.

69. Mallamaci, A., Iannone, R., Briata, P., Pintonello, L., Mercurio, S., Boncinelli, E., and Corte, G. (1998). EMX2 protein in the developing mouse brain and olfactory area. Mech Dev *77*, 165-172.

70. Mahlapuu, M., Ormestad, M., Enerbäck, S., and Carlsson, P. (2001). The forkhead transcription factor Foxf1 is required for differentiation of extra-embryonic and lateral plate mesoderm. Development *128*, 155-166.

71. Lynch, A.T., Phillips, N., Douglas, M., Dorgnach, M., Lin, I.H., Adamson, A.D., Darieva, Z., Whittle, J., Hanley, N.A., Bobola, N.*, et al.* (2025). HAND1 level controls the specification of multipotent cardiac and extraembryonic progenitors from human pluripotent stem cells. EMBO J *44*, 2541-2565.

Langtaosha (LTS) Preprint doi: https://doi.org/10.65215/LTSpreprints.2026.08.25.000317. This version posted August 26, 2026. The copyright holder for this preprint (which was not certified by peer review) is the author/funder. Creative Commons license: CC Attribution-NonCommercial-NoDerivatives 4.0 https://creativecommons.org/licenses/by-nc-nd/4.0

72. Pham, T.X.A., Panda, A., Kagawa, H., To, S.K., Ertekin, C., Georgolopoulos, G., van Knippenberg, S., Allsop, R.N., Bruneau, A., Chui, J.S., *et al.* (2022). Modeling human extraembryonic mesoderm cells using naive pluripotent stem cells. Cell Stem Cell *29*, 1346-1365 e1310.
73. Pijuan-Sala, B., Griffiths, J.A., Guibentif, C., Hiscock, T.W., Jawaid, W., Calero-Nieto, F.J., Mulas, C., Ibarra-Soria, X., Tyser, R.C.V., Ho, D.L.L., *et al.* (2019). A single-cell molecular map of mouse gastrulation and early organogenesis. Nature *566*, 490-495.
74. Miyazono, K., Kamiya, Y., and Morikawa, M. (2010). Bone morphogenetic protein receptors and signal transduction. J Biochem *147*, 35-51.
75. Yu, P.B., Deng, D.Y., Lai, C.S., Hong, C.C., Cuny, G.D., Bouxsein, M.L., Hong, D.W., McManus, P.M., Katagiri, T., Sachidanandan, C., *et al.* (2008). BMP type I receptor inhibition reduces heterotopic [corrected] ossification. Nat Med *14*, 1363-1369.
76. Myers, D.C., Sepich, D.S., and Solnica-Krezel, L. (2002). Bmp activity gradient regulates convergent extension during zebrafish gastrulation. Dev Biol *243*, 81-98.
77. Reversade, B., Kuroda, H., Lee, H., Mays, A., and De Robertis, E.M. (2005). Depletion of Bmp2, Bmp4, Bmp7 and Spemann organizer signals induces massive brain formation in Xenopus embryos. Development *132*, 3381-3392.
78. Hadas, R., Rubinstein, H., Mittnenzweig, M., Mayshar, Y., Ben-Yair, R., Cheng, S., Aguilera-Castrejon, A., Reines, N., Orenbuch, A.-H., and Lifshitz, A. (2024). Temporal BMP4 effects on mouse embryonic and extraembryonic development. Nature *634*, 652-661.
79. Wymeersch, F.J., Wilson, V., and Tsakiridis, A. (2021). Understanding axial progenitor biology in vivo and in vitro. Development *148*.
80. Gouti, M., Metzis, V., and Briscoe, J. (2015). The route to spinal cord cell types: a tale of signals and switches. Trends Genet *31*, 282-289.
81. Kennedy, M.W., Chalamalasetty, R.B., Thomas, S., Garriock, R.J., Jailwala, P., and Yamaguchi, T.P. (2016). Sp5 and Sp8 recruit beta-catenin and Tcf1-Lef1 to select enhancers to activate Wnt target gene transcription. Proc Natl Acad Sci U S A *113*, 3545-3550.
82. Koch, F., Scholze, M., Wittler, L., Schifferl, D., Sudheer, S., Grote, P., Timmermann, B., Macura, K., and Herrmann, B.G. (2017). Antagonistic Activities of Sox2 and Brachyury Control the Fate Choice of Neuro-Mesodermal Progenitors. Dev Cell *42*, 514-526 e517.
83. Cunningham, T.J., Kumar, S., Yamaguchi, T.P., and Duester, G. (2015). Wnt8a and Wnt3a cooperate in the axial stem cell niche to promote mammalian body axis extension. Dev Dyn *244*, 797-807.
84. Liu, A., and Niswander, L.A. (2005). Bone morphogenetic protein signalling and vertebrate nervous system development. Nat Rev Neurosci *6*, 945-954.
85. Ruiz i Altaba, A., Palma, V., and Dahmane, N. (2002). Hedgehog–Gli

Langtaosha (LTS) Preprint doi: https://doi.org/10.65215/LTSpreprints.2026.08.25.000317. This version posted August 26, 2026. The copyright holder for this preprint (which was not certified by peer review) is the author/funder. Creative Commons license: CC Attribution-NonCommercial-NoDerivatives 4.0 https://creativecommons.org/licenses/by-nc-nd/4.0

signaling and the growth of the brain. Nature Reviews Neuroscience *3*, 24-33.
86. Patten, I., and Placzek, M. (2000). The role of Sonic hedgehog in neural tube patterning. Cell Mol Life Sci *57*, 1695-1708.
87. De Robertis, E.M., and Kuroda, H. (2004). Dorsal-ventral patterning and neural induction in Xenopus embryos. Annu Rev Cell Dev Biol *20*, 285-308.
88. Chamberlain, C.E., Jeong, J., Guo, C., Allen, B.L., and McMahon, A.P. (2008). Notochord-derived Shh concentrates in close association with the apically positioned basal body in neural target cells and forms a dynamic gradient during neural patterning. Development *135*, 1097-1106.
89. Besnard, V., Wert, S.E., Hull, W.M., and Whitsett, J.A. (2004). Immunohistochemical localization of Foxa1 and Foxa2 in mouse embryos and adult tissues. Gene Expr Patterns *5*, 193-208.
90. Bachiller, D., Klingensmith, J., Kemp, C., Belo, J.A., Anderson, R.M., May, S.R., McMahon, J.A., McMahon, A.P., Harland, R.M., Rossant, J.*, et al.* (2000). The organizer factors Chordin and Noggin are required for mouse forebrain development. Nature *403*, 658-661.
91. McMahon, J.A., Takada, S., Zimmerman, L.B., Fan, C.-M., Harland, R.M., and McMahon, A.P. (1998). Noggin-mediated antagonism of BMP signaling is required for growth and patterning of the neural tube and somite. Genes & development *12*, 1438-1452.
92. Sylva, M., van den Hoff, M.J., and Moorman, A.F. (2014). Development of the human heart. Am J Med Genet A *164A*, 1347-1371.
93. Paige, S.L., Plonowska, K., Xu, A., and Wu, S.M. (2015). Molecular regulation of cardiomyocyte differentiation. Circ Res *116*, 341-353.
94. Rossi, G., Broguiere, N., Miyamoto, M., Boni, A., Guiet, R., Girgin, M., Kelly, R.G., Kwon, C., and Lutolf, M.P. (2021). Capturing Cardiogenesis in Gastruloids. Cell Stem Cell *28*, 230-240 e236.
95. Yamada, T., Trentesaux, C., Brunger, J.M., Xiao, Y., Stevens, A.J., Martyn, I., Kasparek, P., Shroff, N.P., Aguilar, A., Bruneau, B.G.*, et al.* (2025). Synthetic organizer cells guide development via spatial and biochemical instructions. Cell *188*, 778-795 e718.
96. Tyser, R.C., Miranda, A.M., Chen, C.M., Davidson, S.M., Srinivas, S., and Riley, P.R. (2016). Calcium handling precedes cardiac differentiation to initiate the first heartbeat. Elife *5*, e17113.
97. Potthoff, M.J., and Olson, E.N. (2007). MEF2: a central regulator of diverse developmental programs. Development *134*, 4131-4140.
98. DeLisser, H.M., Christofidou-Solomidou, M., Strieter, R.M., Burdick, M.D., Robinson, C.S., Wexler, R.S., Kerr, J.S., Garlanda, C., Merwin, J.R., Madri, J.A.*, et al.* (1997). Involvement of endothelial PECAM-1/CD31 in angiogenesis. Am J Pathol *151*, 671-677.
99. Krause, D.S., Fackler, M.J., Civin, C.I., and May, W.S. (1996). CD34: structure, biology, and clinical utility. Blood *87*, 1-13.
100. Nowotschin, S., Setty, M., Kuo, Y.-Y., Liu, V., Garg, V., Sharma, R., Simon, C.S., Saiz, N., Gardner, R., and Boutet, S.C. (2019). The emergent landscape

Langtaosha (LTS) Preprint doi: https://doi.org/10.65215/LTSpreprints.2026.08.25.000317. This version posted August 26, 2026. The copyright holder for this preprint (which was not certified by peer review) is the author/funder. Creative Commons license: CC Attribution-NonCommercial-NoDerivatives 4.0 https://creativecommons.org/licenses/by-nc-nd/4.0

of the mouse gut endoderm at single-cell resolution. Nature *569*, 361-367.

101. Ameri, J., Ståhlberg, A., Pedersen, J., Johansson, J.K., Johannesson, M.M., Artner, I., and Semb, H. (2010). FGF2 specifies hESC-derived definitive endoderm into foregut/midgut cell lineages in a concentration-dependent manner. Stem cells *28*, 45-56.

102. Chen, C., Wu, J., Wang, X., Chang, L., Wang, K., Wu, K., Guo, M., Li, H., Sun, F., Jiang, X.*, et al.* (2025). Signaling reprogramming via Stat3 activation unravels high-fidelity human post-implantation embryo modeling. Cell Stem Cell *32*, 1528-1544 e1510.

103. Oura, S., Li, L., and Wu, J. (2025). An inducible model of human post-implantation development derived from primed and naive stem cells. Cell Stem Cell *32*, 1509-1527 e1509.

104. Li, J., Li, J., Cao, J., Shang, S., Zhang, L., Gao, F., Fu, J., Chen, H., Cui, G., Wu, H.*, et al.* (2026). Modelling late gastrulation in stem cell-derived monkey embryo models. Nature *649*, 161-172.

105. Li, J., Zhu, Q., Cao, J., Liu, Y., Lu, Y., Sun, Y., Li, Q., Huang, Y., Shang, S., Bian, X.*, et al.* (2023). Cynomolgus monkey embryo model captures gastrulation and early pregnancy. Cell Stem Cell *30*, 362-377 e367.

106. Zheng, W., Peng, B., Chen, Z., Huang, K., Qi, Y., Niu, H., Shen, H., Wu, J., Jiao, J., and Du, P. (2026). Continuous modeling of primate embryogenesis from totipotency to early organogenesis. Cell *189*, 4664-4684 e4669.

107. Hanna, J., Cheng, A.W., Saha, K., Kim, J., Lengner, C.J., Soldner, F., Cassady, J.P., Muffat, J., Carey, B.W., and Jaenisch, R. (2010). Human embryonic stem cells with biological and epigenetic characteristics similar to those of mouse ESCs. Proceedings of the National Academy of Sciences *107*, 9222-9227.

108. Wu, J., Platero-Luengo, A., Sakurai, M., Sugawara, A., Gil, M.A., Yamauchi, T., Suzuki, K., Bogliotti, Y.S., Cuello, C., and Valencia, M.M. (2017). Interspecies chimerism with mammalian pluripotent stem cells. Cell *168*, 473-486. e415.

109. Lemaire, L., Roeser, T., Izpisua-Belmonte, J.C., and Kessel, M. (1997). Segregating expression domains of two goosecoid genes during the transition from gastrulation to neurulation in chick embryos. Development *124*, 1443-1452.

110. Yang, R., Goedel, A., Kang, Y., Si, C., Chu, C., Zheng, Y., Chen, Z., Gruber, P.J., Xiao, Y., Zhou, C.*, et al.* (2021). Amnion signals are essential for mesoderm formation in primates. Nat Commun *12*, 5126.

111. Perea-Gomez, A., Vella, F.D., Shawlot, W., Oulad-Abdelghani, M., Chazaud, C., Meno, C., Pfister, V., Chen, L., Robertson, E., Hamada, H.*, et al.* (2002). Nodal antagonists in the anterior visceral endoderm prevent the formation of multiple primitive streaks. Dev Cell *3*, 745-756.

112. Simunovic, M., Siggia, E.D., and Brivanlou, A.H. (2022). In vitro attachment and symmetry breaking of a human embryo model assembled from primed embryonic stem cells. Cell Stem Cell *29*, 962-972 e964.

113. Grebenyuk, S., and Ranga, A. (2019). Engineering Organoid

Langtaosha (LTS) Preprint doi: https://doi.org/10.65215/LTSpreprints.2026.08.25.000317. This version posted August 26, 2026. The copyright holder for this preprint (which was not certified by peer review) is the author/funder. Creative Commons license: CC Attribution-NonCommercial-NoDerivatives 4.0 https://creativecommons.org/licenses/by-nc-nd/4.0

Vascularization. Front Bioeng Biotechnol *7*, 39.

114. Palis, J., and Yoder, M.C. (2001). Yolk-sac hematopoiesis: the first blood cells of mouse and man. Exp Hematol *29*, 927-936.

115. Ewels, P., Magnusson, M., Lundin, S., and Kaller, M. (2016). MultiQC: summarize analysis results for multiple tools and samples in a single report. Bioinformatics *32*, 3047-3048.

116. Dobin, A., Davis, C.A., Schlesinger, F., Drenkow, J., Zaleski, C., Jha, S., Batut, P., Chaisson, M., and Gingeras, T.R. (2013). STAR: ultrafast universal RNA-seq aligner. Bioinformatics *29*, 15-21.

117. Stuart, T., Butler, A., Hoffman, P., Hafemeister, C., Papalexi, E., Mauck, W.M., 3rd, Hao, Y., Stoeckius, M., Smibert, P., and Satija, R. (2019). Comprehensive Integration of Single-Cell Data. Cell *177*, 1888-1902 e1821.

118. Korsunsky, I., Millard, N., Fan, J., Slowikowski, K., Zhang, F., Wei, K., Baglaenko, Y., Brenner, M., Loh, P.R., and Raychaudhuri, S. (2019). Fast, sensitive and accurate integration of single-cell data with Harmony. Nat Methods *16*, 1289-1296.

119. Gu, Z., Eils, R., and Schlesner, M. (2016). Complex heatmaps reveal patterns and correlations in multidimensional genomic data. Bioinformatics *32*, 2847-2849.

120. Dai, M., Pei, X., and Wang, X.J. (2022). Accurate and fast cell marker gene identification with COSG. Brief Bioinform *23*, bbab579.